Lithos 380–381 (2021) 105816

Contents lists available at ScienceDirect

Lithos

journal homepage: www.elsevier.com/locate/lithos

Research Article

Protolith-controlled superposition of Sn-(W) and Cu-Mo mineralization: Examples from the Jurassic and Cretaceous granite-related mineralization in the coastal region of southeastern China

Wenting Huang [a], Huaying Liang [a,*], Long Ren [a], Xilian Chen [b], Jian Zhang [c], Kaixuan Li [b]

[a] CAS Key Laboratory of Mineralogy and Metallogeny, Guangzhou Institute of Geochemistry, Chinese Academy of Sciences, Guangzhou 510640, China
[b] State Key Laboratory of Nuclear Resources and Environment, East China University of Technology, Nanchang 330013, China
[c] Key Laboratory of Environment Change and Resources Use in Beibu Gulf, Ministry of Education, Nanning Normal University, Nanning 530004, China

ARTICLE INFO

Article history:
Received 17 June 2020
Received in revised form 30 September 2020
Accepted 2 October 2020
Available online 8 October 2020

Keywords:
Granite-related ores
Porphyry deposit
Crustal melting
Mesozoic
South China

ABSTRACT

Sn (W) and Cu-Mo have distinct geochemical behaviors during magmatic evolution, thus these two group deposits are seldom superposed. Specially, the Mesozoic granite-related Sn-*W*/W-Sn and Mo-Cu/Cu-Mo deposits in south China are spatial overlapped, with some are even temporal-coincided. To reveal the factors controlling the distribution and the locally coeval occurrence of different mineralization types, here we compared the ages, sources compositions, and tectonic settings of the Jurassic Zijinshan Sn-rich granite, the Jurassic Gutian porphyry Mo-Cu deposit, and the Cretaceous Luoboling porphyry Cu-Mo deposit from the southeastern (SE) China. The results indicate that the Jurassic Sn-W and Mo-Cu rich magmas were derived from Paleoproterozoic metasedimentary and meta-basaltic rocks, respectively, through partial melting (>850 °C) along the suture zones triggered by asthenospheric upwelling in the intra-plate extensional setting. The Cretaceous porphyry Cu-Mo deposit was formed by water-flux melting (<800 °C) of the mantle wedge metasomatized by the fluids derived from the subducted Paleo-Pacific plate. A protoliths-controlled distribution model was proposed, namely that during Jurassic, the suture zones, where were the ancient continental margins containing both metasedimentary and meta-basaltic rocks, favored heat input from upwelling mantle and high temperature melting, which consumed the both protoliths to form W-Sn and Mo-Cu rich magmas in the same region; shift in tectonic setting from intra-plate extension to subduction during Cretaceous, introduced mantle or juvenile crust-derived materials to source, therefore formed Cu-Mo deposits superposing the Jurassic W-Sn and Mo-Cu ores in SE China.

1. Introduction

The ore elements Cu, Au, Mo, and Sn-(W) have distinct geochemical behaviors in felsic magmatic and hydrothermal processes (Williams-Jones and Heinrich, 2005; Richards, 2011); therefore, felsic igneous rock related Cu, Au, Mo, and Sn-(W) mineralizations are formed by different means, i.e., different source rocks, magmatic oxidization states, and magmatic compositional evolution paths; thus, they are related to distinct tectonic settings (Ishihare, 1981; Richards, 2011; Romer and Kroner, 2016).

For instance, Cu, and to a lesser extent Mo, are derived from the mantle (Audétat, 2010; Richards, 2011) and tend to be concentrated in oxidized magmas (Liang et al., 2006; Sun et al., 2013), and are transported into the shallow crust by hydrothermal fluids to form mineralization. Subducted slabs contribute metals, volatile fluxes, and oxidizing elements and compounds to the overriding asthenopspheric mantle (Richards, 2003; Sillitoe, 2010), where partial melting during subduction (Mitchell and Garson, 1981), or post-subduction thermal adjustments (Hou et al., 2003; Richards, 2009) form magmas that favor porphyry Cu and Mo mineralization. Therefore, Cu and Mo mineralizations usually develop at active plate boundaries (Cooke et al., 2005; Hollings et al., 2005; Sillitoe, 2010). Some porphyry deposits, especially the large Mo deposits, have been formed in intraplate environments, most of which were likely controlled by extensional zones or deep fault systems (Huang et al., 2017a; Mao et al., 2013).

Sn-(W) mineralization involves the presence of sedimentary protoliths, heat sources to drive partial melting of the protoliths, and subsequent high degrees of fractionation of a reduced magma (Lehmann, 2004; Romer and Kroner, 2015, 2016). Several researchers have suggested that separated linear belts of Cu-Mo and Sn-W mineralizations were affected by subduction, and that the different types of mineralization were due to the different distances of the belts from the trench (Sillitoe, 1972), or due to differences in the angle of the subducting slab with depth (Mitchell, 1973). However, Sn-(W) mineralization also occurs in a wide range of tectonic settings, such as back arc basins (Garson

* Corresponding author.
E-mail address: lianghy@gig.ac.cn (H. Liang).

https://doi.org/10.1016/j.lithos.2020.105816
0024-4937/

and Mitchell, 1977), continental collision zones (Mitchell and Garson, 1981), and settings unrelated to active plate margins (Sillitoe, 1974). Thus, rather than a specific tectonic setting, the essential requirement for the formation of Sn-(W) mineralization is a former continental margin, which has been reworked by crustal extension and rifting and has ample heat inputs (Romer and Kroner, 2015, 2016).

Since Cu, Au, Mo, and Sn-(W) mineralizations are controlled by distinct geochemical processes, Cu, Au, Mo, and Sn-(W) mineralization belts generally have distinct spatial distributions, and when they spatially coincide, they are not generally coeval (Lehmann, 2004; Romer and Kroner, 2015, 2016).

Mesozoic magmatism widely occurred in southern China and formed many metallogenic belts/regions with various metal associations and heterogeneous distributions (Hu and Zhou (2012); Mao et al., 2013). For example, the Jurassic Sn-W metallogenic province in the Nanling Range, as well as the Cretaceous porphyry-epithermal Cu-Au-Mo metallogenic belt in the coastal region of southeastern (SE) China, were formed in a back-arc extensional setting (Hu and Zhou, 2012; Mao et al., 2013) and in an active continental margin subduction setting, respectively (Jiang et al., 2013; Wang et al., 2013; Huang et al., 2018).

In the last decade, Jurassic porphyry Mo-Cu and granite-related Sn-(W) deposits have been found in the coastal region of SE China, thus attracting increasing amounts of attention (Fig. 1; Supplemental Table 1). Unlike the spatial separation of most Sn-(W) and Cu-Mo mineralizations around the world, these Jurassic deposits coincide spatially and temporally. For instance, the newly discovered Gutian Mo-Cu porphyry deposit is located ~60 km north of the Zijinshan (ZJS) Sn-mineralized granites (Fig. 1), which are located in the ZJS Cretaceous epithermal-porphyry Cu-Au-Mo ore field. The key factors controlling the simultaneous formation of granite-related deposits with distinct elemental associations within the same area remain unknown. Furthermore, whether these coastal Jurassic Sn-(W) and Mo-Cu deposits formed above an active continental margin, i.e., similar to the tectonic setting of the Cretaceous Cu-Au-Mo mineralization in the region, or were formed in a tectonic background similar to that of the Jurassic Nanling Sn-W metallogenic province inland, is still unclear.

In this study, we determined zircon U-Pb and molybdenite *Re*-Os ages, analyzed the zircon- trace element and Hf isotopic composition, and determined the whole-rock major and trace element composition and Sr-Nd isotopic compostion of ore related felsic igneous rocks, together with previous published data, we compare the Jurassic intrusions of the Gutian porphyry Mo-Cu deposit, the Jurassic ZJS Sn-mineralized granite, and the Cretaceous Luoboling Cu-Mo porphyry in the Zijinshan ore field (ZOF) in terms of their ages, magmatic sources, oxidation states, petrogenesis, and tectonic backgrounds. The goal of this study is to investigate the reasons for the spatial coincidence of simultaneous or diachronous Sn-W and Mo-Cu/Cu-Mo mineralization in SE China, which provides insight into the metallogenic evolution of southern China.

2. Regional Geology

The South China Block (SCB) consists of the Yangtze Block and the Cathaysia Block (Fig. 1a), which were amalgamated during the Neoproterozoic along the NE-trending Shi-Hang fault zone (Chen and Jahn, 1998; Shen, 2006). The Cathaysia Block is further divided into the western and eastern terranes on the two sides of the NE-trending crustal Zhenghe-Dapu fault (Fig. 1b) (Chen and Jahn, 1998; Xu et al., 2007). The Cathaysia Block has a widespread Paleoproterozoic basement composed of metamorph volcano-sedimentary, sedimentary, and igneous rocks (Xu et al., 2007). The MORB-like amphibolites (1.77–1.85Ga), and the gneissic granite suits with S-type and A-type affinities (1.83–1.89 Ga) define a Paleoproterozoic orogenic cycle in the Cathaysia Block (Li et al., 2000; Xia et al., 2012; Yu et al., 2009).

Multiple periods of magmatism, including Neoproterozoic (~850 Ma), Paleozoic (~450–250 Ma), and Mesozoic (~90–190 Ma) events, occurred in the SCB (Li et al., 2013; Xu et al., 2007). In particular, in the Cathaysia Block, the large-scale Mesozoic magmatism formed a large granite province covering an area of more than 100,000 km^2 (Li and Li, 2007; Sun, 2006; Zhou and Li, 2000).

The Jurassic igneous rocks mainly occur in the hinterland and consist of S-type granites (peraluminous granites), some I-type granites, and subordinate A-type granites (Zhou and Li, 2000; Zhou et al., 2006). The large scale Sn-W deposits associated with the Jurassic peraluminous granites are located in the intra-continental region (Fig. 1, Supplemental Table 1), especially in the Nanling district (Fig. 1b) (Chen et al., 2016; Zhang et al., 2006). The SCB also contains Jurassic porphyry-skarn Cu-Mo-(±Au) deposits, which are mainly located within the Shi-Hang deep-fault zone (Mao et al., 2013; Hu and Zhou, 2012; Huang et al., 2017a; Zhou and Li, 2000). Hinterland extension during Jurassic, which was triggered by asthenosphere upwelling, was suggested to cause the widespread crustal melting, the formation of a large granitic province, and the Sn-W metallogenesis in the Nangling Range (Hu and Zhou, 2012; Yuan et al., 2019). However, the geodynamic mechanism for the hinterland extension remains controversial, that including intra-plate rifting (Gilder et al., 1991; Li, 2000; Wang et al., 2008), mantle plumes (Xie et al., 1996), and subduction of the Paleo-Pacific Plate (Mao et al., 2013; Zhou and Li, 2000; Zhou et al., 2006; Li and Li, 2007; Sun et al., 2007).

In the southeastern (SE) China, the Jurassic intrusions are sporadic (Wang et al., 2012), whose associated Sn-W deposits (such as Shangfa and Xingluokeng) and porphyry Mo-Cu deposit (such as Gutian) have been found along the Zhenghe-Dapu fault recently (Fig. 1). The Cretaceous magmatism resulted in a large NE-SW trending magmatic belt in the SE China (Zhou et al., 2006). This magmatic belt contains large scale volcanics and some granites, which are mainly of metaluminous (Guo et al., 2012; Zhou and Li, 2000). The Cretaceous magmatism is mainly associated with porphyry Cu-Mo or epithermal Au-polymetallic deposits (Mao et al., 2013), such as the Zijinshan porphyry-epithermal Cu-Au-Mo deposit (Jiang et al., 2013; So et al., 1998) and the Zhilingtou epithermal Au-Ag deposit (Wang et al., 2016). The Mesozoic magmatism in the SE China, which formed several Jurassic intrusions as well as widespread Cretaceous igneous rocks, was triggered by the subduction and roll back of the Paleo-Pacific Plate (Guo et al., 2012; Li and Li, 2007; Li et al., 2014; Zhou and Li, 2000; Zhou et al., 2006).

3. Ore deposit geology

3.1. Geologic setting of the ZOF

The strata in the ZOF are mainly comprised of Neoproterozoic low grade metamorphic shallow-marine clastic sediments, Late Devonian and Early Carboniferous coastal to shallow-marine clastic sediments, and the volcanic rocks and the Quaternary alluvial sediments of the Early Cretaceous Shimaoshan Group (Fig. 2). The intrusions in the ZOF were mainly emplaced in the Middle to Late Jurassic and Early Cretaceous (ca. 165 Ma to ca. 93 Ma, Jiang et al., 2013; Zhang et al., 2001).

The Jurassic intrusions include the Zijinshan (ZJS) granite complex and the Caixi monzogranite. The ZJS granite complex outcrops in the central part of the ore field with an area of ~18 km^2 (Fig. 2); it includes the Jingmei coarse grained granite, the Wulongsi medium-fine grained granite, and the Jinlongqiao fine grained granite. The complex has U-Pb zircon ages of 157 ± 1 Ma to 165 ± 1 Ma (Jiang et al., 2013). The ~90 km^2 Caixi monzogranite, which is located in the northeastern part of the ore field, has a U-Pb zircon age of 150 ± 3 Ma (Zhao et al., 2007). Some of the greisen- and quartz vein-type Sn mineralization is reported to have a close spatial relationship with the Wulongsi medium-fine grained grainte (Fig. 4a) (Zhang et al., 2001), suggesting that the Sn mineralization is genetically related to the Jurassic granites

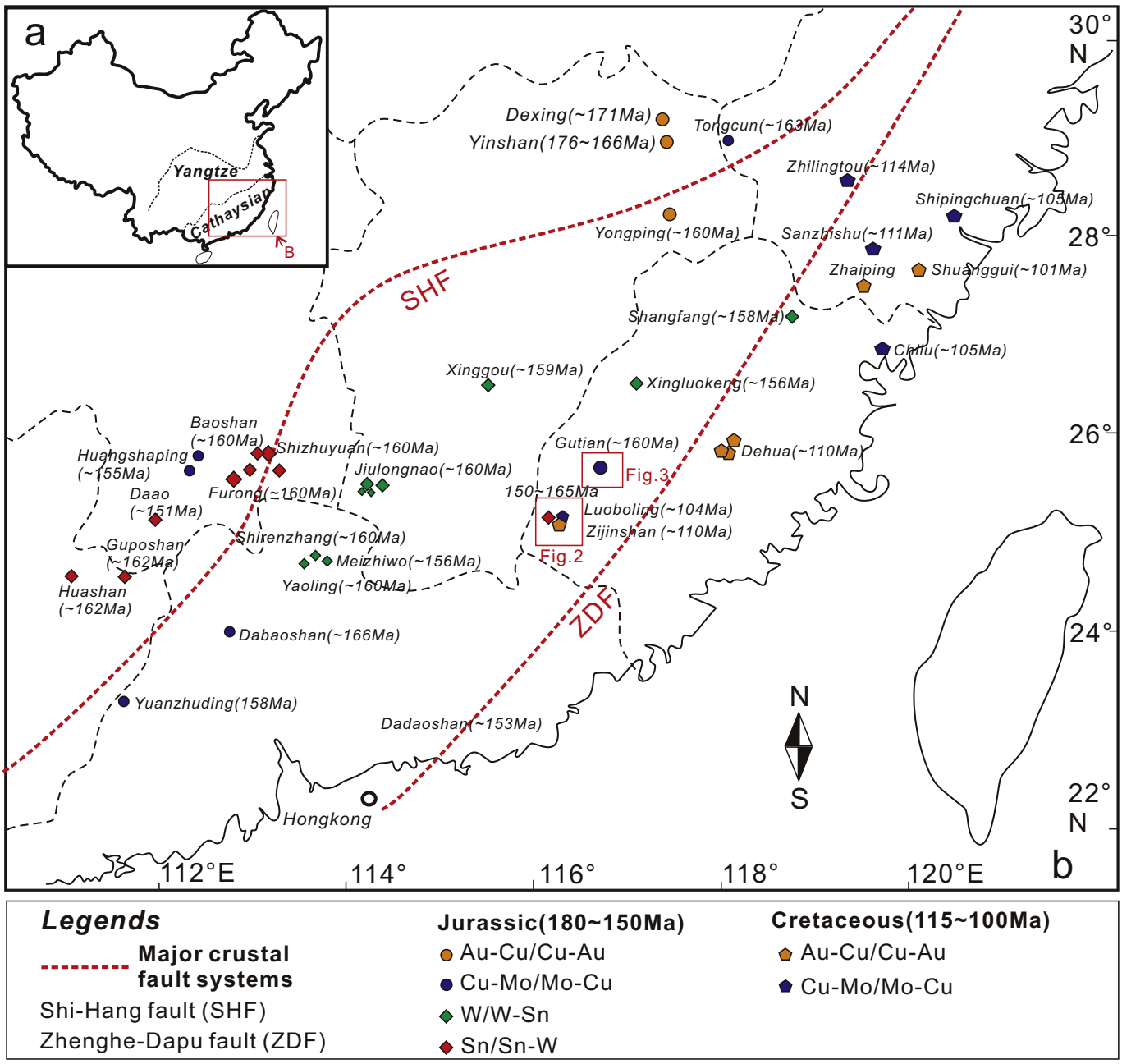

Fig. 1. Simplified geologic map of southern China showing the distribution of the Middle-Late Jurassic (180–150 Ma) and Early Cretaceous (115–100 Ma) rocks. Data sources are the same as in Supplemental Table 1.

(Liu et al., 2016; Zhang et al., 2001).Given that the granite-related Sn mineralization mostly occurs at the top of the intrusions (Heinrich, 1990; Linnen, 1998), the large outcrop surface of the Jurassic granites is in the ZOF, and they underwent large scale denudation, the original scale of the Sn deposit was larger than the present size of the deposit.

Cretaceous intrusions occur widely in the ZOF, including the Sifang granodiorite (U-Pb zircon age of 112 ± 1 Ma) (Jiang et al., 2013) and the Luoboling granodiorite porphyry (U-Pb zircon age of ca. 103 Ma) (Huang et al., 2018).

A series of deposits related to Cretaceous magmatism have been found in the ZOF and have an estimated metallic resource of 399 tons of Au, 6339 tons of Ag, 4.14 million tons of Cu, and 0.11 million tons of Mo (Zhang, 2013). From the east to the west, they are the Luoboling large Cu-Mo porphyry deposit, the Wuziqilong small-scale epithermal Cu-Ag-Au deposit, the Zijinshan giant high-sulfidation epithermal Au-Cu deposit, the Jinmei small-scale Cu-Mo porphyry deposit, the Longjiangting large intermediate-sulfide epithermal Cu-Ag-Au deposit, and the Yueyang large low-sulfidation Ag-Au-Cu deposit (Fig. 2). The Luoboling Cu-Mo porphyry deposit is genetically related to the Luoboling granodiorite porphyry, which is composed of plagioclase, quartz, biotite, and hornblende phenocrysts within a groundmass of quartz, K-feldspar, plagioclase, and biotite (Fig. 4b). The ore minerals are mainly pyrite, chalcopyrite, and molybdenite, with minor amounts of bornite, digenite, and magnetite (Huang et al., 2013; Zhong et al., 2014).

3.2. Geologic setting of the Gutian Mo-Cu porphyry deposit

The Gutian Mo-Cu porphyry deposit is located about 60 km northeast of the ZOF. The outcrops in the area are dominated by Holocene sediments. The Gutian deposit contains multiple stages of intrusions,

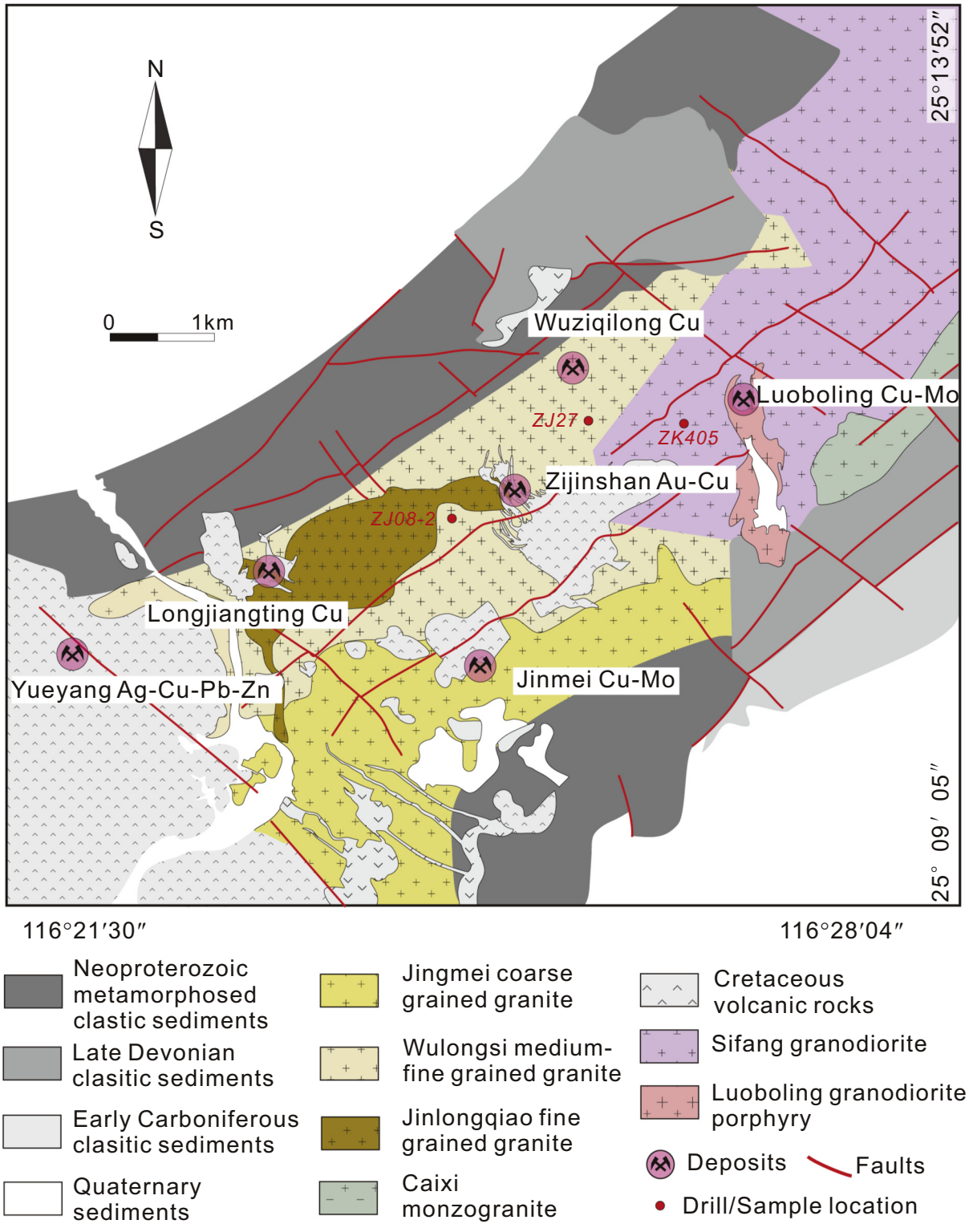

Fig. 2. Geologic map of the Zijinshan ore field (modified after Zhong et al., 2014).

forming a magmatic complex with an outcrop area of ~20 km^2 (also the Kuokeng complex; Li et al., 2016a). Form early to late, the intrusions are monzogranite, granodiorite, granodiorite porphyry, and tonalite dikes. The Mo-Cu mineralization is mainly hosted in the granodiorite and granodiorite porphyry (Fig. 3). The granodiorite is composed of feldspar, quartz, amphibole, and biotite (Fig. 4c). The granodiorite porphyry is composed of plagioclase (30 vol%), K-feldspar (10 vol%), amphibole (10 vol%), biotite (~10 vol%), and quartz (~5 vol%) phenocrysts and a fine-grained groundmass with a similar mineral association (Fig. 4e). The ores predominantly occur as veinlets, with minor amounts of disseminated mineralization in the granodiorite and granodiorite porphyry. The metallic minerals mainly include chalcopyrite, molybdenite, and pyrite (Fig. 4d, f). The gangue minerals are quartz, sericite, K-feldspar, and chlorite (Li et al., 2016b).

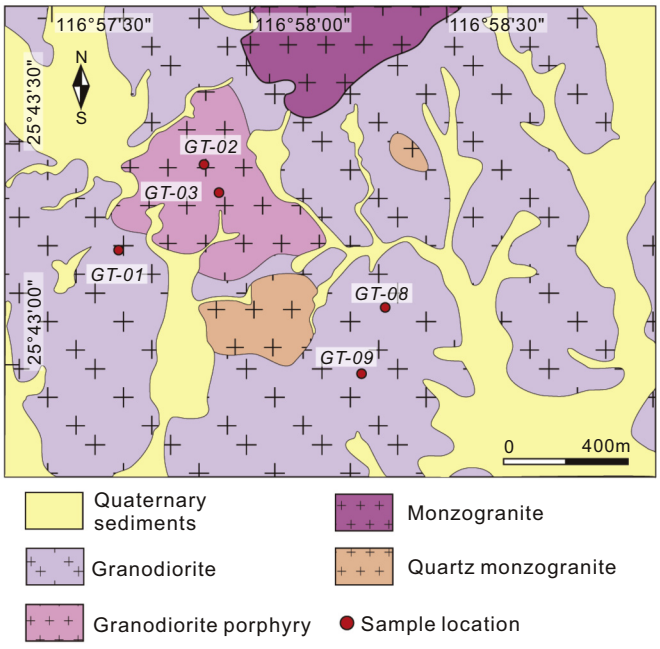

Fig. 3. Geologic map of the Gutian Mo-Cu porphyry deposit (modified after Li et al., 2016a).

4. Analytical Methods and results

Detailed analytical methods, zircon trace elements and U-Pb dating, molybdenite *Re*-Os isotopic compositions, whole rock geochemical and Sr-Nd isotopic compositions, and zircon Lu-Hf isotopic compositions are given in Supplemental Materials. The results are presented in Supplemental Tables 2–7. A summary of the results is presented in Table 1.

4.1. Zircon U-Pb ages and trace element compositions

The zircon U-Pb isotopic data are presented in Supplemental Table 2. Their trace element compositions are presented in Supplemental Table 3. Representative zircon CL images are shown in Fig. 5.

4.1.1. Luoboling granodiorite porphyry

Twenty-five zircon grains from sample LBL-95 were selected for analysis. They yielded U-Pb ages of 98.2 ± 1.6 Ma to 146.5 ± 2.3 Ma. One zircon with an anomalous age of 146.5 ± 2.3 Ma was interpreted to be an inherited zircon. On the cumulative probability plot, the three points at the extremes of the range indicate possible Pb loss (98.2 ± 1.6 Ma) or inheritances (109.2 ± 2.0 Ma and 107.5 ± 2.0 Ma). When these points are excluded, the rest 20 zircon grains yield a weighted mean age of 103.8 ± 0.6 Ma (MSWD =0.74; Fig. 5a). These zircon grains are characterized by weak Eu anomalies (with Eu_N/Eu^* ratios of 0.5–0.7, Supplemental Table 3). They also exhibit high Ce^{4+}/Ce^{3+} ratios of 415–1486 (mean of 878), suggesting the melt was oxidized (Fig. 6, Supplemental Table 3).

4.1.2. Wulongsi medium-fine grained granite

The zircon grains from sample ZJ08-2 are euhedral and exhibit oscillatory zoning in the CL images, suggesting a magmatic origin. Twenty-six zircon grains were selected for U-Pb dating, yielding Th/U ratios of 0.28–2.0. Of the 26 analytical spots, 19 spots have correlations in $^{206}Pb/^{238}U$ versus $^{207}Pb/^{235}U$ > 90% with $^{206}Pb/^{238}U$ ages of 135.0 ± 2.7 to 843 ± 22.4 Ma (Supplemental Table 2). Two zircon grains with ages of 375 ± 7.8 Ma and 843 ± 22.4 Ma are inherited, whereas five grains with ages of <154 Ma plot below the concordia, indicating that they experienced Pb loss. The rest 12 zircon grains yielded a weighted mean age of 169.3 ± 3.3 Ma (MSWD = 1.4; Fig. 5b). These zircon grains are enriched in HREEs, with strong Eu negative anomalies (Eu_N/Eu^* = 0.18–0.43) and low Ce^{4+}/Ce^{3+} ratios (17–178), indicating the melt was reduced.

Twenty-five zircon grains from sample ZJ-27 were analyzed. Twenty-three of the grains with correlations in $^{206}Pb/^{238}U$ versus $^{207}Pb/^{235}U$ > 90% have Th/U ratios of 0.25–1.70 and $^{206}Pb/^{238}U$ ages of 142.6 ± 4.2 to 199.0 ± 3.9 Ma (Supplemental Table 2). Four of the zircon grains with ages of 185.4 ± 4.5 to 199.0 ± 3.9 Ma, and four with ages of 142.6 ± 4.2 to 152.0 ± 4.0 Ma, are attributed to inheritance and loss, respectively, since they plot above and below the concordia. The 14 zircon grains have a weighted mean age of 168.7 ± 4.0 Ma (MSWD = 2.9; Fig. 5c). These zircon grains have similar geochemical composition with those from sample ZJ08-2, that exhibit strong Eu negative anomalies with low Ce^{4+}/Ce^{3+} ratios (Supplemental Table 3).

4.1.3. Gutian granodiorite

Twenty five zircon grains from sample GT-01 were analyzed. Fifteen of the grains were inherited and have U-Pb ages of 756.9 ± 14.2 to 203.6 ± 9.8 Ma. The rest 10 zircon grains have U-Pb ages of 149.2 ± 5.3 to 174.6 ± 10.2 Ma, with a weighted mean age of 164.4 ± 5.4 Ma (MSWD = 1.9, Fig. 5d). The 10 Jurassic zircon grains are characterized by weaker Eu negative anomalies (Eu_N/Eu^* = 0.49–0.70) and higher Ce^{4+}/Ce^{3+} ratios (255–1435) (Fig. 6) compared with those of the grains from the Wulongsi medium-fine grained granite.

4.1.4. Gutian granodiorite porphyry

Sample GT-02 included 10 inherited zircon grains with U-Pb ages of 427.6 ± 8.3 to 194.3 ± 5.6 Ma. The rest 15 spots had U-Pb ages of 170.2 ± 4.9 to 154.5 ± 5.2 Ma and a weighted mean age of 162.3 ± 2.9 Ma (MSWD = 1.3, Fig. 5e).

Twenty-five zircon grains from sample GT-03 were analyzed. Thirteen of the grains were inherited, with U-Pb ages of 470.6 ± 15.5 to 204.5 ± 11.4 Ma. The rest 12 zircon grains have U-Pb ages of 170.7 ± 5.0 to 154.1 ± 4.0 Ma, with a weighted mean age of 161.8 ± 2.9 Ma (MSWD = 1.7, Fig. 5f).

The 27 Jurassic zircon grains from the granodiorite porphyry are geochemically similar to those of the Gutian granodiorite. They have weak negative Eu anomalies (averaged Eu_N/Eu^* = 0.47) and a mean Ce^{4+}/Ce^{3+} ratio of 558 (Fig. 6, Supplemental Table 3), indicating the melts were relatively oxidized.

4.2. Molybdenite Re-Os isotopic composition

The molybdenite Re-Os isotopic compositions of three samples from the Gutian porphyry Mo-Cu deposit are presented in Supplemental Table 4 and are shown in Supplemental Fig. 1.

The molybdenite samples have very low Re concentrations of less than 1.0 ppm. They contain 531.0–152.4 ppb of ^{187}Re and 1.4–0.4 ppb of ^{187}Os, model ages of 151.3 ± 0.6 Ma to 153.9 ± 3.9 Ma, and a weighted mean age of 151.6 ± 1.6 Ma (MSWD = 0.86). Three of the samples yielded an isochron age of 155 ± 18 Ma (MSWD = 0.11).

4.3. Whole-rock major and trace element compositions

The new bulk-rock geochemical data for the Luoboling granodiorite porphyry, the Gutian granodiorite, and the Gutian granodiorite porphyry obtained in this study, as well as the previously published data for these intrusions (Li et al., 2014; Li et al., 2016a, 2016b) and for the Zijinshan granite complex (Li et al., 2015), are presented in Supplemental Table 5 and Figs. 7 and 8.

The Luoboling porphyry plots in the andesite field on the $Na_2O + K_2O$ vs. SiO_2 (TAS) diagram (Fig. 7a), and they have a high-K calc-alkaline affinity according to the K_2O vs. SiO_2 diagram (Fig. 7b). They have metaluminous affinity with molar $Al_2O_3/(CaO + Na_2O + K_2O)$ (A/CNK) ratios of 0.88–0.99 (Fig. 7c). These samples are enriched in large ions lithophile elements (LILEs), such as Rb, Sr, and Ba, are

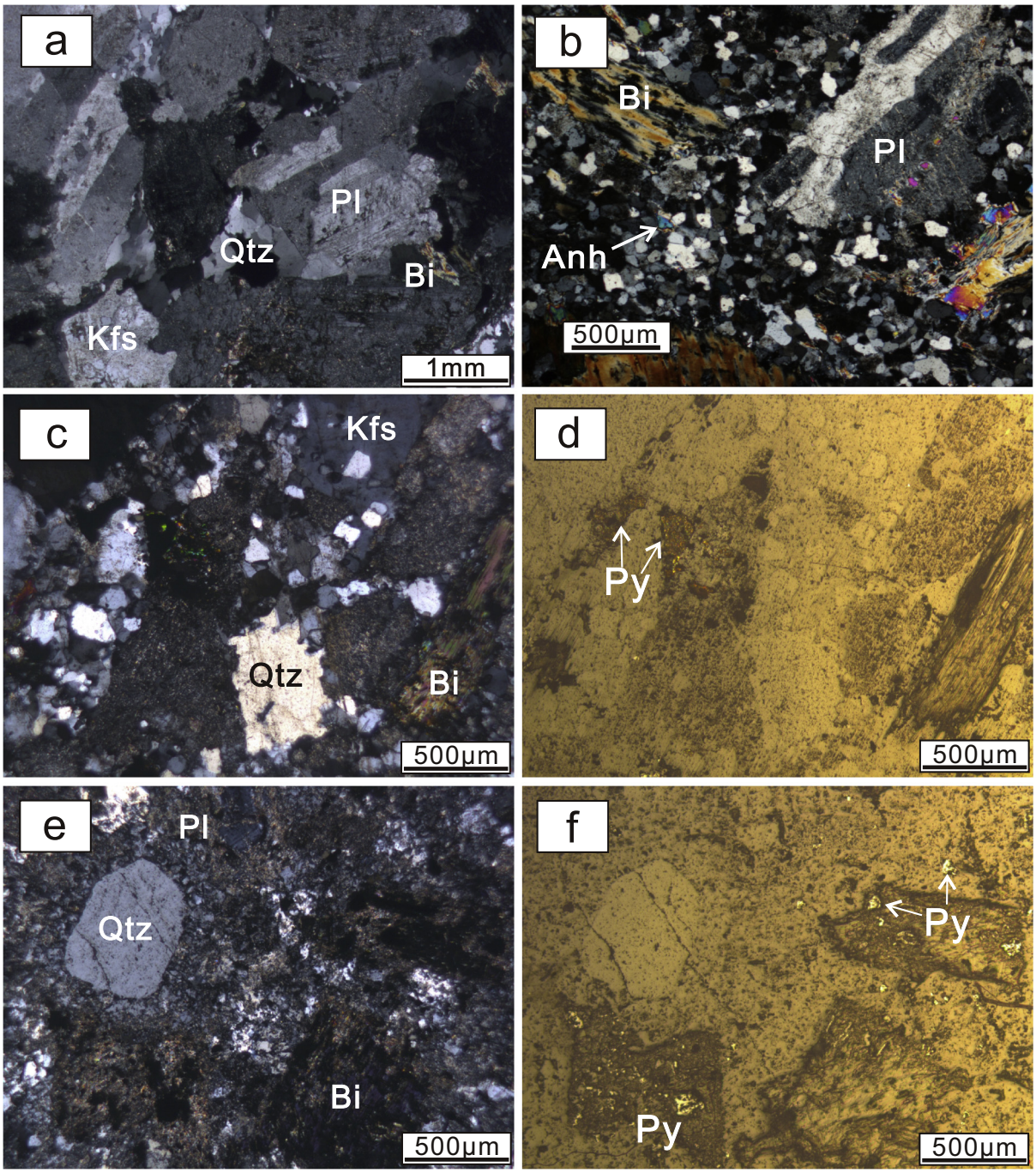

Fig. 4. Photomicrographs showing the mineral assemblages of representative samples from (a) the Jurassic Zijinshan granite, (b) the Luoboling granodiorite porphyry, (c, d) the Jurassic Gutian granodiorite, and (e, f) the granodiorite porphyry. Abbreviations: Hbl = hornblende, Bi = biotite, Kfs = K-feldspar, Pl = plagioclase, Qtz = quartz, Anh = anhydrite.

depleted in high field strength elements (HFSEs), such as Nb, Ta and Y (Fig. 8a), and have Sr/Y ratios higher than 30.0 (average of 33.3). Their zircon saturation temperature (T_{Zr}) was calculated to be 722–791 °C following the method of Watson and Harrison (1983). Their chondrite-normalized REEs patterns exhibit a moderate enrichment in light rear earth elements (LREEs) over heavy rear earth elements (HREEs), and weak negative Eu anomalies (Fig. 8b), with $[La/Yb]_N$ mean of 14.6 and Eu_N/Eu^* values mean of 0.90.

The ZJS granite complex is characterized by high SiO_2 concentrations (>70 wt%) and peraluminous affinity (A/CNK = 1.0 to 3.4), that plots within the rhyolite/granite field on the TAS diagram (Fig. 7a). The granite complex has very low CaO (mostly <0.30 wt%), MgO (<0.40 wt%), Fe_2O_3 (mostly <1.5 wt%) contents, and relatively low Nb/Ta (⟨10) and Sr/Y ratios (mostly <10). The Jinmei coarse grained granite and the Jinlongqiao fine grained granite have similar trace element compositions (Fig. 8c). They exhibit weak enrichments in LREEs over HREEs ($[La/Yb]_N$ = 4.4–11.4) (Fig. 8d) and negative Eu anomalies in chondrite-normalized REEs patterns, and have T_{Zr} of 709–837 °C. The medium-fine grained Wulongsi granite has ∑REE contents, $(La/Yb)_N$ and Eu_N/Eu^* ratios that are substantially lower than those of the Jinmei and Jinglongqiao granites (Table 1, Supplemental Table 5), which characterized by a tetrad chondrite-normalized REE pattern (Fig. 8d). It is also characterized by lower T_{Zr} (703–728 °C) compared to the other two granite phases.

Table 1
Summary of Geochemistry Features for the Luoboling Granodiorite Porphyry, Zijinshan Granite Complex, and Gutian Intrusions.

Lithology	Age (Ma)	Whole rock						Zircon				Data source
		SiO_2 (wt%)	A/CNK	Nb/Ta	Sr/Y	T_{Zr}(°C)	$\varepsilon_{Nd}(t)$	T_{DM}(Ga)	$\varepsilon_{Hf}(t)$	Ce^{4+}/Ce^{3+} (Range/average)	Eu_N/Eu^* (Range/average)	
Luoboling Porphyry												
Granodiorite Porphyry	103	61.30–65.85	0.88–0.99	8.76–12.4	29.9–36.2	722–791	−2.8 – −5.1	0.95–1.28	−1.6 – −3.7	210–2621	877 ± 498 (n = 30)	0.42–0.77	0.58 ± 0.09 (n = 30)	This study; Li et al., 2015
Zijinshan Granite Complex												
Carose Grained	164	75.04–78.54	1.00–1.28	4.05–6.43	1.75–6.76	709–837	−6.6 – −8.5	1.50–1.63	−7.1 – −9.7					This study; Li et al., 2015
Middle-Fine Grained	163	76.50–77.85	1.08–1.21	4.38–5.25	4.02–6.54	703–728	−6.7 – −8.0	1.50–1.59	−7.6 – −11.8	4–178	69 ± 52 (n = 68)	0.15–0.38	0.28 ± 0.07 (n = 68)	
Fine Grained	155	75.59–79.89	2.27–3.35	5.90–8.90	7.68–28.0	786–814	−9.3 – −10.3	1.70–1.78	−8.1 – −13.9					
Gutian Intrusions												
Granodiorite Gorphyry	158–162	63.81–67.88	0.93–1.16	10.3–13.6	22.2–53.8	802–846	−8.5 – −12.5	1.64–1.97	−9.0 – −16.3	61–2475	558 ± 514 (n = 26)	0.27–0.98	0.47 ± 0.17 (n = 26)	This study, Li et al., 2016a; Li et al., 2016b
Granodiorite	164	67.00–70.88	0.97–1.12	10.2–15.3	29.1–34.1	780–843	−7.8 – −9.4	1.58–1.71	−8.4 – −15.2	255–1435	699 ± 330 (n = 10)	0.34–0.68	0.52 ± 0.11 (n = 10)	
Quartz-Monzorite	161	54.85–66.32	0.96–1.02	11.9–13.0	26.5–35.0	816–841	−8.7 – −9.4	1.66–1.72						

The Gutian granodiorite has slightly higher SiO_2 concentrations than those of the granodiorite porphyry and the quartz monzonite (Supplemental Table 5). These intrusions plot in the granodiorite and quartz-monzonite fields on the TAS diagram (Fig. 7a), and plot in the high-K calc-alkaline field on the K_2O vs. SiO_2 diagram (Fig. 7b). They are mostly exhibit a metaluminous affinity with A/CNK ratios of 0.93–1.16 (Fig. 7c). They also have similar trace-element compositions that exhibit enrichment in LILEs and Pb, and depletion in HFSEs and Ti (Fig. 8e). They have relatively high Sr/Y ratios of 22.2–53.8 (average of 34.5), and relatively high T_{Zr} of 780–846 °C. Their normalized REEs exhibit a listric pattern, a moderate enrichment in LREEs over HREEs (with $[La/Yb]_N$ = 11.4–22.2, Fig. 8f), and weak negative Eu anomalies (Eu_N/Eu^* = 0.80–1.06).

4.4. Whole-rock Sr-Nd isotopic compositions

The results of the Rb-Sr and Sm-Nd isotopic analyses of the Luoboling porphyry conducted in this study combined with the published Sr-Nd isotopic data for the Luoboling granodiorite porphyry (Li et al., 2014), the ZJS granite complex (Li et al., 2015), and the Gutian intrusions (Li et al., 2016a, 2016b) are presented in Supplemental Table 6 and Figs. 9 and 10a.

The $(^{87}Sr/^{86}Sr)_i$ values of the Luoboling granodiorite porphyry are of 0.7066 to 0.7077 (Fig. 9). The $\varepsilon_{Nd}(t)$ values range from −2.8 to −5.1 (Fig. 10a), and the corresponding two stage model ages (T_{DM2}) range from 0.95 Ga to 1.28 Ga.

The Jinmei coarse grained granite samples have high Rb/Sr ratios of up to 8.5, and therefore their variable and low $(^{87}Sr/^{86}Sr)i$ values (0.7017 to 0.7051) are not taken into account. The rest of the samples from the ZJS granite complex have consistently high $(^{87}Sr/^{86}Sr)_i$ values of 0.7095 to 0.7132. The Jinmei granite and the Wulongsi granite have similar $\varepsilon_{Nd}(t)$ values of −6.8 to −8.5 and −6.7 to −8.0, respectively, with T_{DM} ranging from 1.5 to 1.6 Ga. The Jinlongqiao fine grained granite has slightly lower $\varepsilon_{Nd}(t)$ ratios of −9.3 to −10.3, with T_{DM2} from 1.7 to 1.8 Ga.

The granodiorite, granodiorite porphyry, and quartz monzonite from the Gutian have consistent $(^{87}Sr/^{86}Sr)_i$ values of 0.7088 to 0.7092, 0.7085 to 0.7096, and 0.7088 to 0.7097, respectively. Most of these samples yielded identical $\varepsilon_{Nd}(t)$ ratios of −8.4 to −9.7, with T_{DM2} values of 1.6 to 1.7 Ga.

4.5. Zircon Hf isotopic compositions

The results of the zircon Hf isotopic compositions for the Luoboling granodiorite porphyry and the Gutian granodiorite porphyry are presented in supplemental Table 7 and Fig. 10b.

Fifteen zircon grains from the Luoboling granodiorite porphyry (LBL-95) yielded $^{176}Hf/^{177}Hf$ ratios of 0.282606–0.282693 and ε_{Hf} (t) values of −0.6 to −3.7 (calculated using the weighted mean U-Pb age of 103 Ma). These zircon grains have associated T_{DM2} of 1202 to 1397 Ma.

Thirteen zircon grains from the Gutian granodiorite porphyry (GT-03) yielded $^{176}Hf/^{177}Hf$ ratios of 0.282214–0.282391 and ε_{Hf} (t) values of −10.0 to −16.3 (calculated using the weighted mean U-Pb age of 160 Ma). These zircon grains have associated T_{DM2} of 1841 to 2237 Ma.

5. Discussion

5.1. Timing of the Jurassic metallogenesis in the coastal region of SE China

Previous studies have reported that the ZJS granite complex was emplaced 169–149 Ma (Jiang et al., 2013; Zhao et al., 2007). Some of the greisen-type and quartz vein-type Sn mineralization have a close spatial relationship to the Wulongsi granite (Zhang et al., 2001); thus, it has been suggested that they are genetically linked (Liu et al., 2016). Geochemically, the Wulongsi granite exhibits a tetrad REE pattern

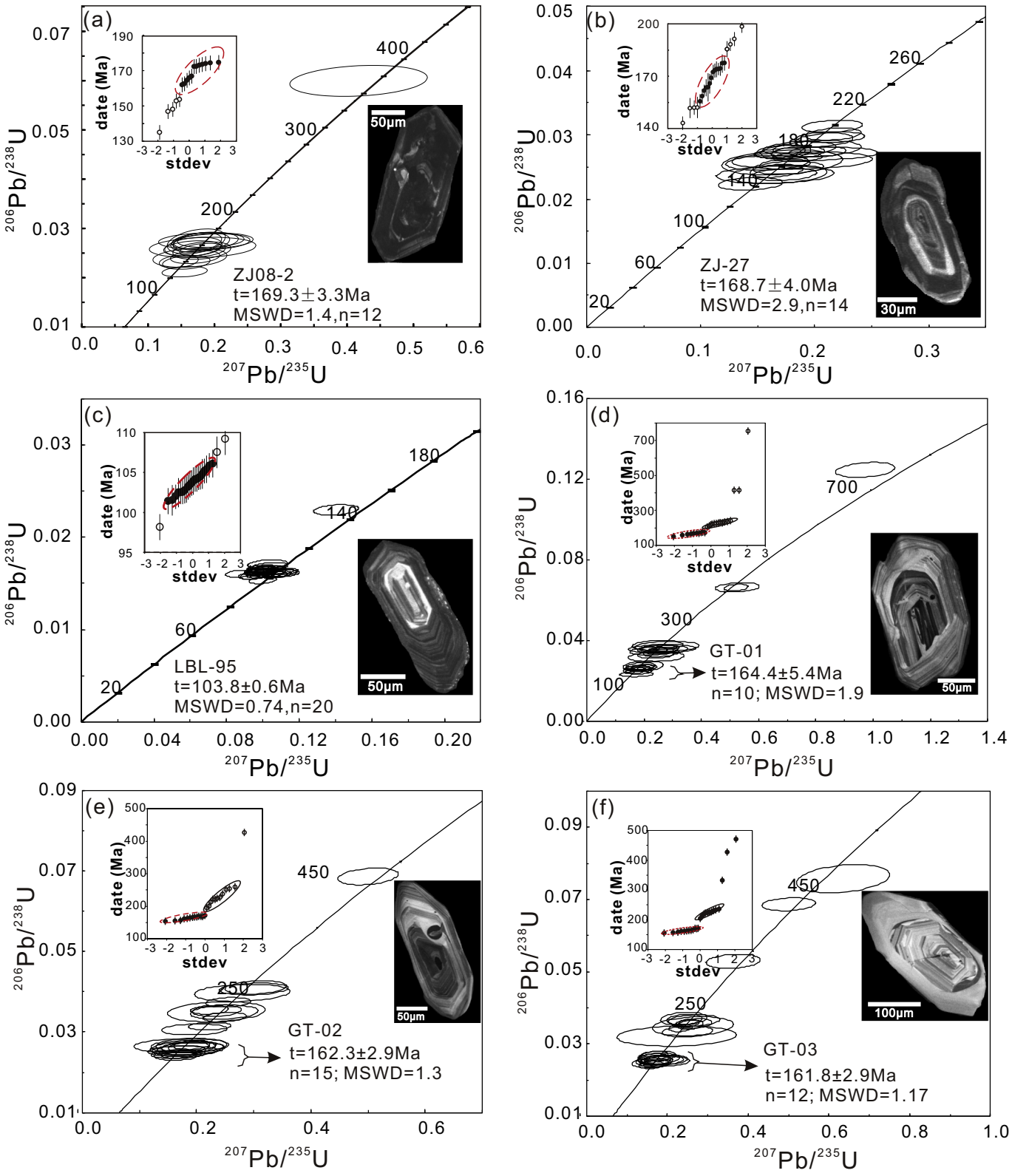

Fig. 5. CL images of representative zircon grains and LA-ICP-MS zircon U-Pb concordia diagrams for representative samples from the ZJS granite, the Luoboling granodiorite porphyry, the Gutian granodiorite, and the granodiorite porphyry. The insets are the cumulative probability plots.

(Fig. 8d) (Li et al., 2015), which is indicative of the interaction between granitic melts and magmatic fluids (Huang et al., 2017b; Irber, 1999; Monecke et al., 2002). This feature further supports the hypothesis that the Wulongsi granite gave rise to the Sn mineralization in the ZOF. Our new U-Pb zircon ages for the Wulongsi granite (169.3 ± 3.3 Ma to 168.7 ± 4.0 Ma) are within error of previously published ages (168.0 ± 4.0 Ma to 163.3 ± 4.0 Ma) (Jiang et al., 2013; Li et al., 2015; Yu et al., 2013), suggesting that the Jurassic magmatic rocks

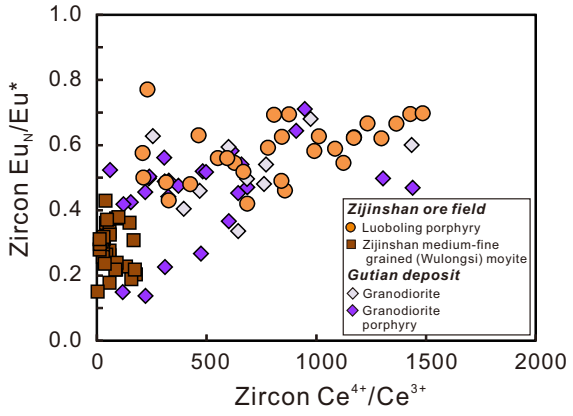

Fig. 6. Plot of zircon Eu_N/Eu^* ratio vs. zircon Ce^{4+}/Ce^{3+} ratio for the ZJS granite, the Luoboling granodiorite porphyry, and the Gutian intrusions.

associated with the Sn mineralization in the ZOF were emplaced ~163–169 Ma.

The Gutian Mo-Cu porphyry deposit is newly discovered and has attracted considerable attention (Li et al., 2016a, 2016b). Our U-Pb zircon ages for the mineralized granodiorite and granodiorite porphyry (164.4 ± 5.4 Ma and 161.8 ± 2.9 to 162.3 ± 2.9 Ma, respectively) agree well with published U-Pb zircon ages of the granodiorite porphyry (158.4 ± 1.8 Ma to 161.4 ± 1.3 Ma) and granodiorite (164.1 ± 1.8 Ma) as well as the *Re*-Os model ages of the molybdenite from the granodiorite porphyry (162.4 ± 2.7 Ma and 163.0 ± 2.3 Ma) (Li et al., 2016a, 2016b). Together, these data indicate that the magmatism and the related Mo-Cu mineralization of the Gutian deposit occurred at about 161–164 Ma.

The molybdenite from the quartz-pyrite-molybdenite vein hosted in the granodiorite porphyry yielded consistent Re-Os isochron ages (155 ± 18 Ma) and mean model ages (151.6 ± 1.6 Ma), which are contemporaneous with the age of the youngest mineralized granodiorite porphyry in the Gutian deposit (U-Pb zircon age of 158.4 ± 1.8 Ma; Li et al., 2016a) within error. These data suggest that the late episode magmatism in Gutian also caused the mineralization at ~155 Ma.

We propose that two stages of Mo-Cu mineralization occurred in the Gutian deposit. The early stage occurred at ~165–162 Ma, and the late stage occurred at ~155 Ma. These ages overlap with the ages of the ZJS Sn-mineralized granite and are similar to those of the recently discovered Sn-W deposits in southeastern China, such as the Xingluokeng W ± Sn deposit (molybdenite Re-Os age of 156.3 ± 4.8 Ma; Zhang et al., 2008), the Shangfang W deposit (molybdenite Re-Os age of 158.1 ± 5.4 Ma; Chen et al., 2013), and the Dadaoshan Sn deposit (molybdenite Re-Os age of 152.6 ± 1.8 Ma; Qiu et al., 2017) (Fig. 1). Based on the close spatiotemporal relationships between these Jurassic deposits (Fig. 1), we conclude that they constitute an episode of Jurassic felsic rock related metallogenesis in the coastal region of SE China, which caused both the Sn-W and Mo-Cu mineralization.

5.2. Factors controlling the diverse Jurassic Sn and Mo-Cu mineralization in the coastal region of SE China

The Jurassic ZJS granites are characterized by high SiO_2 (Fig. 7), Al_2O_3 (ACNK>1.1), Isr (0.7095–0.7132) values, un-radiogenic whole-rock Nd ($\varepsilon_{Nd}(t) = -6.7$ to -10.3) and zircon Hf ($\varepsilon_{Hf}(t) = -7.1$ to -19.0) isotopes, and low zircon Ce^{4+}/Ce^{3+} ratios (mean of 69, Table 1). They are interpreted to be reduced S-type granites derived from the Paleoproterozoic crust (T_{DM2} = 1660 to 2130 Ma) (Jiang et al., 2013; Li et al., 2015). Their low molar CaO/Na_2O and $CaO/(MgO + FeO_T)$ ratios and high $Al_2O_3/(MgO + FeO_T)$ ratios further indicate a metasedimentary protolith (Figs. 11a, b) (Beard and Lofgren, 1991; Sylvester, 1998). Although the Mo-Cu mineralized intrusions in the Gutian deposits have Nd ($\varepsilon_{Nd}(t) = -7.8$ to -12.5) and zircon Hf ($\varepsilon_{Hf}(t) = -10.0$ to -16.3) isotopes similar to those of the ZJS granite, which are consistent with a crustal derivation, they are metaluminous (Fig. 7c), oxidized (with Ce^{4+}/Ce^{3+} ratios >600), and have lower I_{sr} ratios (0.7085–0.7097) (Fig. 9) and higher CaO contents (Supplemental Fig. 2) than the ZJS granite, implying a distinct meta-basaltic protolith (Fig. 11).

These variations in protolith composition may be the primary factor causing the diverse Sn mineralization in the ZJS and the Mo-Cu in Gutian. The weathered continental sediments are usually enriched in Sn (Romer and Kroner, 2016), and trend to form reduced melts (Sato et al., 2004) in which cassiterite is highly soluble (Linnen et al., 1995), thereby benefiting subsequent Sn-minerlization. On the other hand, the meta-basaltic rocks were mantle-derived ultimately that would relatively enriched in Cu (Rudnick and Gao, 2003; Sun et al., 2013). Partil melting of meta-basaltic rocks would lead to oxidized magmas (Sato et al., 2004) that destabilize the sulfides, thereby promoting magmatic Cu-Mo enrichment and mineralizaiton (Jugo, 2009; Liang et al., 2009; Sun et al., 2013; Zou et al., 2017).

Moreover, the magmas of the ZJS Sn granites and the Gutian Mo-Cu granites underwent different evolutionary paths, which could also be responsible for their distinct element associations. The ZJS granites experienced high degrees of fractional crystallization, as indicated by high SiO_2 contents, Nb/Ta of <10 (Table 1) and tetrad REE patterns (Fig. 8d). Given Sn is incompatible during fractionation (Zajacz et al.,

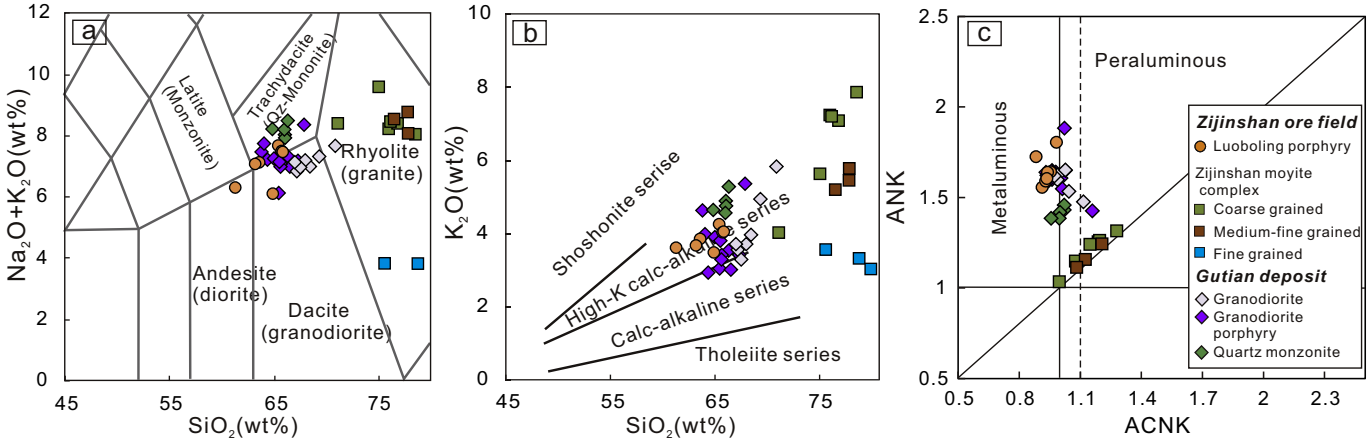

Fig. 7. Plots of (a) $K_2O + Na_2O$ vs. SiO_2 (wt%), (b) K_2O vs. SiO_2 (wt%), and (c) A/NK vs. A/CNK.

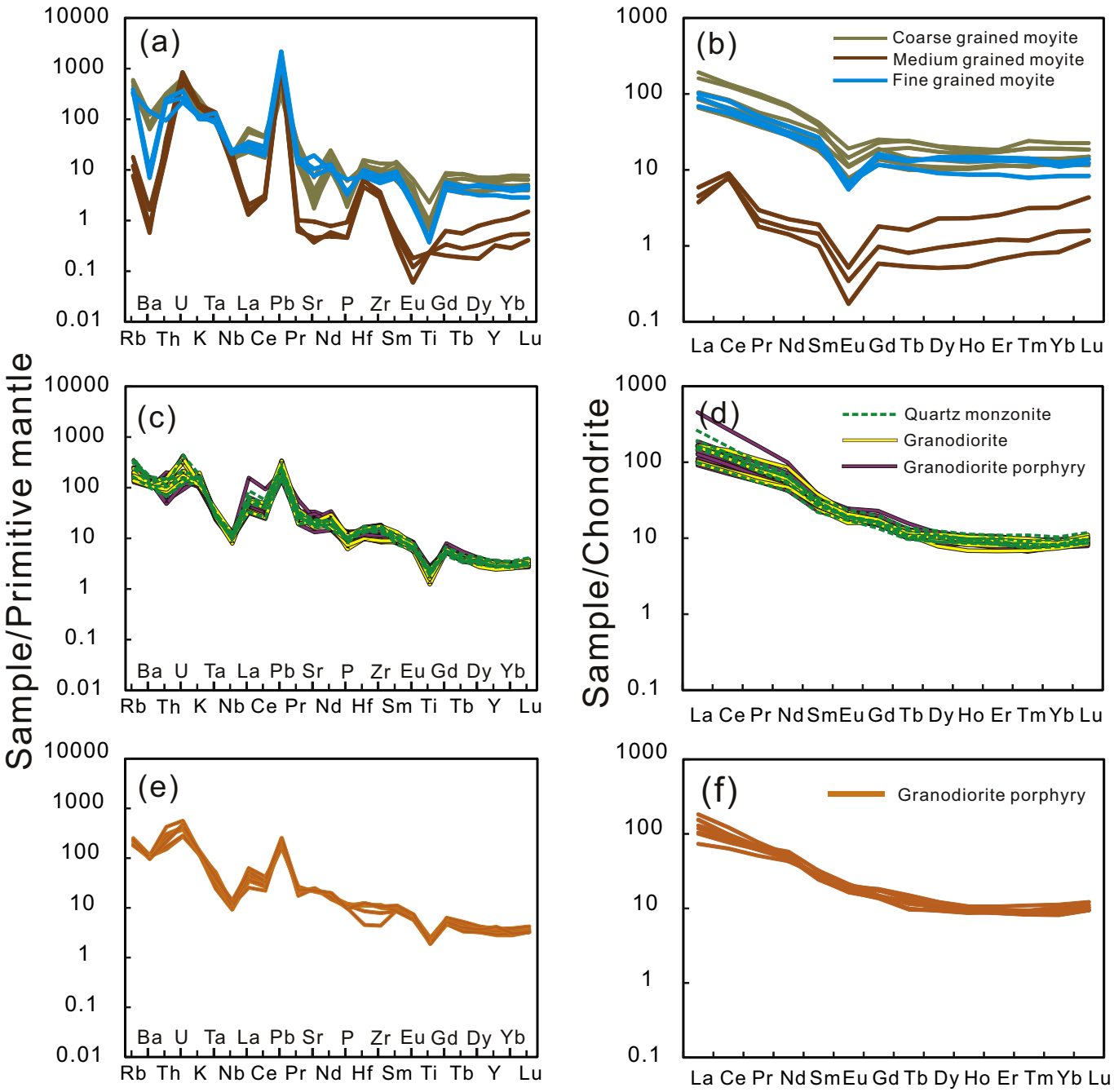

Fig. 8. (a, c, e) Primitive mantle-normalized trace elemental patterns and (b, d, f) chondrite-normalized REE patterns for (a, b) the Luoboling porphyry, (c, d) the ZJS granite complex, and (e, f) the Gutian granodiorite and granodiorite porphyry. The primitive mantle and chondrite normalized values are from McDonough and Sun, 1995.

2008), high degrees of fractional crystallization would concentrate Sn in the residual melts, thereby producing economically viable Sn mineralization (Thomas et al., 2000, 2005; Thomas and Davidson, 2013). The Gutian intrusions are less evolved than the ZJS granites, but their magmas were hydrous based on their high Sr/Y ratios and weak negative Eu anomalies (Table 1, Supplemental Fig. 2), which are consistent with plagioclase suppression and substantial amphibole fractionation in a wet magma (Richards et al., 2012). Such a hydrous magma would favor fluid exsolution and metal extraction from the melt, which would favor the formation of Mo-Cu porphyry deposits (Richards et al., 2012; Wang et al., 2017).

5.3. Tectonic setting and model for the spatial-temporal coupling of the Sn and Mo-Cu mineralizations

In addition to an enriched protolith, the heat source is another key factor controlling the formation and spatial distribution of intrusion-related mineralization (Romer and Kroner, 2015, 2016). We calculated zircon saturation temperatures (Tzr) (Watson and Harrison, 1983) of 709–845 °C and 780–846 °C for the ZJS Sn granite and the Gutian Mo-Cu mineralized intrusions, respectively (Table 1, Fig. 12). The differences in these temperatures may reflect the variable degrees of fractional crystallization of the samples, which is supported by a systematic decrease in

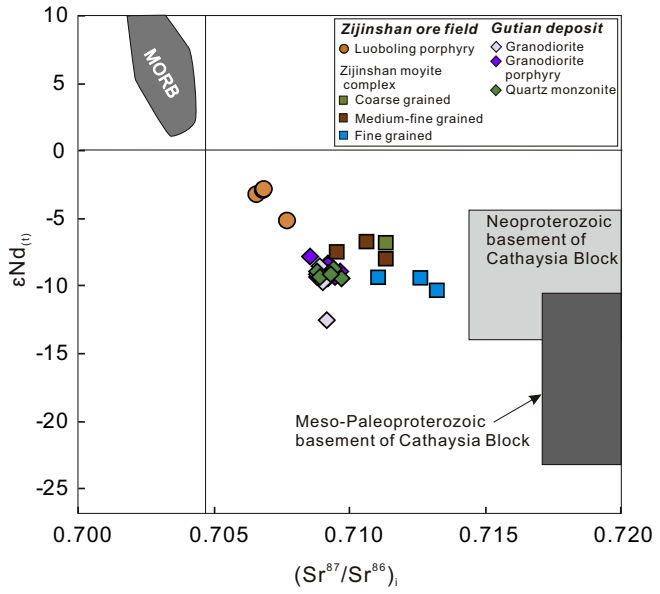

Fig. 9. Plot of initial $^{87}Sr/^{86}Sr$ vs. $\varepsilon_{Nd}(t)$ for the Luoboling granodiorite porphyry, the ZJS granite complex, and the Gutian intrusions. Symbols and references are as in Fig. 8. The fields for the Neoproterozoic low mature basement and the Meso-Paleoproterozoic low mature basement of the Cathaysia Block are from Shen, 2006; and Jiang et al., 2013.

temperature with decreasing Nb/Ta ratio (Fig. 12). Therefore, the least evolved samples of the ZJS granites and Gutian intrusions best represent the melting temperatures (Yuan et al., 2019), both of which are interpreted to be ~850 °C (Fig. 12). High temperatures (>800 °C) are essential for anhydrous melting of hydrous mafic minerals (such as biotite and amphibole) as well as the breakdown of magnetite, titanite, and rutile at crustal pressures (Weinberg and Hasalová, 2015). Therefore, these high temperatures (~850 °C) were favorable for melting the meta-basaltic protoliths of the Gutian intrusions and favored the formation of the Sn-rich magmas of the ZJS granites by consuming the Sn-rich minerals (e.g., biotite, magnetite, titanite, and rutile) in the weathered sedimentary protolith and subsequently releasing Sn into the melts. We conclude that high temperature crustal melting, which simultaneously melted the metasedimentary and meta-basaltic rocks in the crust, is the key factor that produced the locally superimposed granite-related Sn and Mo-Cu porphyry mineralization in the coastal region of SE China.

High temperature crustal melting requires a heat input from the mantle (Clark et al., 2011), which can be accomplished by the intrusion of mantle melts in subduction or extensional zones, or by the emplacement of ultrahigh-temperature metamorphic rocks within an orogenic belt (Romer and Kroner, 2015, 2016). However, the ultrahigh-temperature metamorphic model cannot explain the ZJS granite and the Gutian intrusions since there was no collisional orogenic event in the SE China during the Jurassic. Several researchers have suggested that the SE China was a continental arc formed by the subduction of the Paleo-Pacific Plate in the Jurassic, and that the area was dominated by a compressional regime (Jiang et al., 2013; Li et al., 2016a). However, the sources of the ZJS granite and the Gutian intrusions do not contain mantle or down-going slab derived materials. In fact, several lines of evidence indicate that the coastal region of SE China was controlled by an extensional regime: (Audétat, 2010) Middle Jurassic rift-type basins were widely developed in SE China (Gilder et al., 1991; Shu et al., 2004); (Beard and Lofgren, 1991) bimodal volcanic rocks with U-Pb zircon ages of ~168–139 Ma are well preserved in the Fujian and Guangdong provinces (Guo et al., 2012); and (Chen et al., 2008) Middle-Late Jurassic OIB-like mafic rocks have been found in Fujian Province (Zhou et al., 2006).

The Jurasic large granitic province and related W-Sn metallogenesis in the Nangling Range was formed in hinterland extensional setting that triggered by asthenosphere upwelling (Hu and Zhou, 2012; Huang et al., 2015; Yuan et al., 2019). The following points should be noted. (Audétat, 2010) The Jurassic W-Sn and Mo-Cu mineralizations in the coastal region of SE China are in close proximity to and were coeval with the W-Sn mineralization in the Nanling Range (~160–150 Ma) (Fig. 1, Table 1). (Beard and Lofgren, 1991) The ZJS granites, the Gutian intrusions, and most of the W-Sn granites in the Nanling Range have similar sources and were mainly derived from the Paleoproterozoic-Neoproterozoic basement of the western Cathaysia Block (Table. 1, Fig. 1, and Fig. 10). (Chen et al., 2008) The Sn specific granites in the Nanling Range were formed by high temperature melting (>800 °C) due to the heat from the mantle upwelling through the Shi-Hang lithospheric fault system (Yuan et al., 2019).

Based on the observations discussed above, we suggest that the coastal region of SE China had a hinterland extensional setting similar to that of the Nanling Range during the Jurassic (Chen et al., 2008; Huang et al., 2015; Li, 2000; Li and Li, 2007; Wang et al., 2013). The upwelling mantle could have provided sufficient heat for the crustal melting in the coastal region. Similar to the Shi-Hang fault in the Nanling Range, the Zhenghe-Dapu crustal fault may have acted as an excellent path for mantle heat transport, thereby promoting high temperature (>800 °C) melting in proximal areas and the formation of both the Sn-rich ZJS granite and the Mo-Cu-rich Gutian intrusions.

We conclude that the Jurassic deposits, in both the coastal region of SE China and the Nanling Range, are products of widespread crustal melting driven by heat from the upwelling mantle. Shi-Hang and

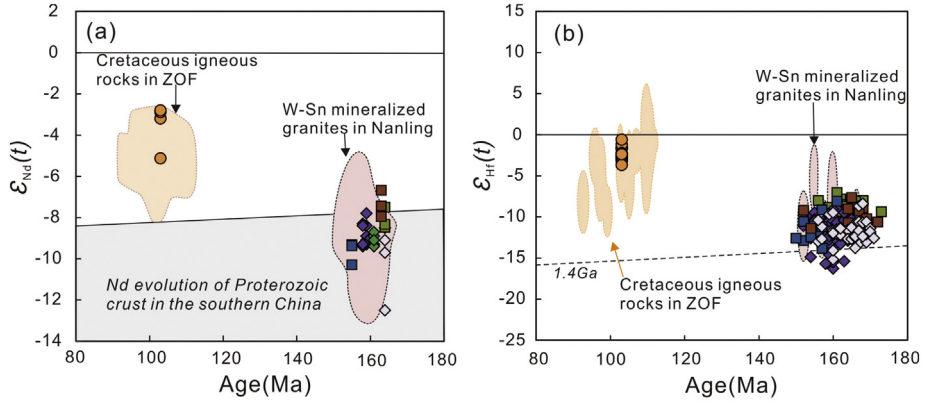

Fig. 10. Plots of (a) $\varepsilon_{Nd}(t)$ vs. age (Ma) and (b) zircon $\varepsilon_{Hf}(t)$ vs. age (Ma). Igneous rock data for the coastal region are from Li et al. (2014, and references therein) and Guo et al. (2012). The symbols and references are as in Fig. 8. Data source of the Sn-W mineralized granites in the Nanling Range is listed in Supplemental Table 1.

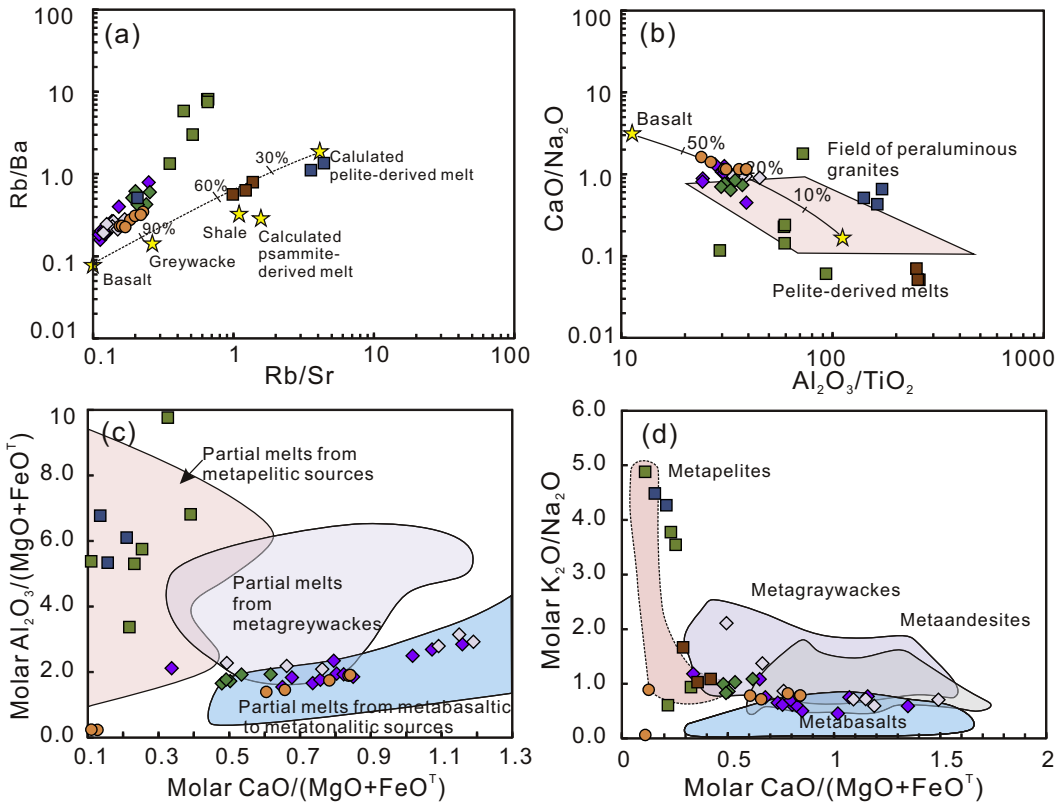

Fig. 11. Plots of (a) Rb/Ba vs. Rb/Sr, (b) CaO/Na_2O vs. Al_2O_3/TiO_2, (c) molar $Al_2O_3/(MgO + FeO_T)$ vs. $CaO/(MgO + FeO_T)$, and (d) molar K_2O/Na_2O vs. $CaO/(MgO + FeO_T)$ for the ZJS granite, the Luoboling porphyry, and the Gutian intrusions. Symbols and references are same as in Fig. 8.

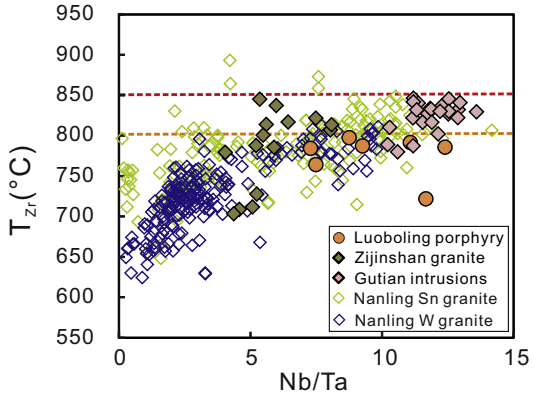

Fig. 12. Plot of zircon saturation temperatures vs. Nb/Ta ratios for the Luoboling granodiorite porphyry, the ZJS granite complex, and the Gutian intrusions. The data for the Nanling Sn and W granites are from Yuan et al. (2019).

Zhenghe-Dapu fault systems were the ancient suture zones of Yangtz-Cathaysia Blocks, and western-eastern Cathaysia terranes (Chen and Jahn, 1998; Xu et al., 2007; Zhang et al., 2008), respectively. As the former continent margins with the development of basins and horsts, Paleoproterozoic arc magams would dominate in the horsts, whereas sedimentary rocks would dominate in the basins, which formed meta-sedimentary and meta-basaltic protoliths in the the basement around the suture zones. On the other hand, these crustal or lithospheric fault systems provided channels for heat transport from the mantle and increased the local crustal geothermal gradient (Fig. 13a). The region proximal to the deep fault systems may have experienced high temperature melting (>800 °C), which would have consumed the biotite and amphibole in the source of the Sn/Sn-W deposits and a few of the Mo-Cu deposits. The region farther away from the deep fault systems would have had a lower geothermal gradient, which caused crustal melting at temperatures of less than 800 °C. Thus, instead of biotite and amphibole, muscovite-controlled anhydrous melting would have dominated under these low temperature conditions, which released the W from the protolith and formed the W-deposits (Yuan et al., 2019). Together, these Jurassic deposits form an EW-trending polymetallic mineralization belt, which is located away from the subduction zone and is controlled by the hinterland extensional setting.

5.4. Tectonic transition-controlled changes in mineralization from the Jurassic to the cretaceous

Most researchers suggest that the SE China was controlled by a subduction setting associated with the westward subduction of the Paleo-Pacific Plate during the Cretaceous (Li et al., 2014; Li and Li, 2007; Wang et al., 2013; Zhou and Li, 2000; Zhou et al., 2006). Due to the tectonic transition, the source components and heat source of the Cretaceous magmatism were distinct from those of the Jurassic magmatism.

The Cretaceous Luoboling Cu-Mo mineralized porphyry is oxidized (Fig. 6), and characterized by more radiogenic Nd (with $\varepsilon_{Nd}(t) = -2.9$ to -5.1) and zircon Hf isotopes (with $\varepsilon_{Hf}(t) = -0.6$ to -3.7) than those of the Jurassic ZJS Sn granites and Gutian Mo-Cu intrusions (with $\varepsilon_{Nd}(t) = -6.7$ to -12.5 and $\varepsilon_{Hf}(t) = -7.1$ to -19.0, Fig. 9). This suggests that the Cretaceous source contained more mantle or juvenile crust-derived materials, which had a higher potential for forming Cu-rich melts rather than Sn-W-rich or high Mo/Cu melts. The Cretaceous Luoboling porphyry has zircon saturation temperatures of <800 °C and Ti-in-zircon temperatures of less than 650 °C, which are significantly lower than the temperatures required for dehydration melting (>850 °C; Collins et al., 2016). This suggests that the source

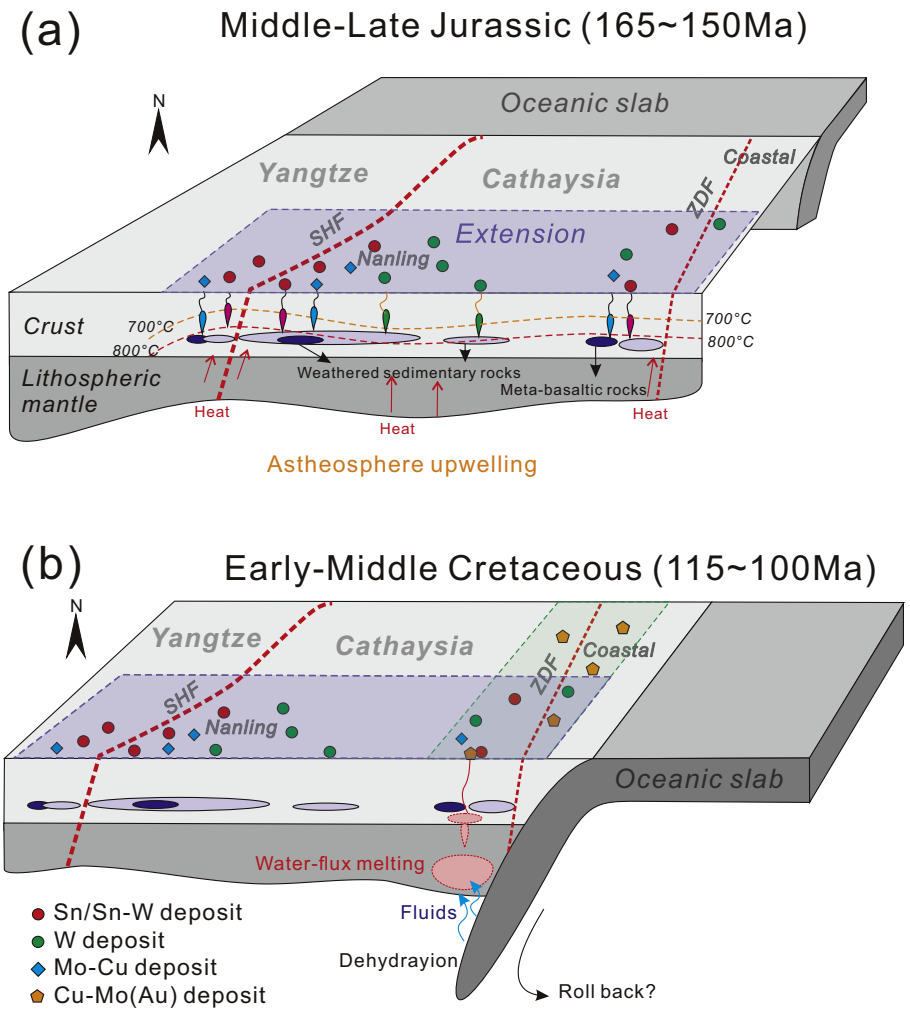

Fig. 13. Model depicting the generation of (a) the Jurassic Sn-W and Mo-Cu deposits in the Nanling Range and the coastal region of SE China, and (b) the Cretaceous Cu-Mo-(Au) mineralization in the coastal region of SE China. The distributions of the Paleproterozoic meta-sedimentary and meta-basalt in crust are not to scale. The widely distribution of Paleproterozoic meta-sedimentary rocks is based on the fact that the granites derived from Paleproterozoic basement are widely occurred in SCB. The distribution of Paleproterozoic meta-basalt is inferred from the distribution of Paleproterozoic suture zones (Shi-Hang and Zhenghe-Dapu faults). The suture zones represent the ancient subduction zone or rift system, where should have developed mafic rocks.

was melted under water-flux conditions (Wang et al., 2017), likely in the metasomatized mantle wedge, which is rich in fluids derived from the down-going slab (Fig. 13b). Water flux melting favors the formation of hydrous and oxidized magmas. Such magmas achieve fluid exsolution before significant fractional crystallization occurs, which enriches the melt in incompatible Mo over compatible Cu (Li and Audétat, 2012), leading to the formation of porphyry deposits with high Cu/Mo ratios. This hypothesis is consistent with the fact that the Cretaceous Luoboling Cu-Mo porphyry underwent lower degrees of fractional crystallization than the Jurassic Gutian Mo-Cu mineralized intrusions, which is supported by the fact that the former lacks tight correlations between SiO_2 and most of the oxides (Supplemental Fig. 2), and that the SiO_2 contents of the former are lower than those of the later.

Overall, the transition in the tectonic setting of the SE China, i.e., controlled by hinterland extension during the Jurassic and a subduction zone during the Cretaceous, caused changes in the magmatic source components, physical-chemical conditions of magma generation, and the magmatic composition. These changes resulted in systematic changes in the predominant mineralization from Sn-W and Mo-Cu to Cu-Mo-(Au), which partially spatially overlap (such as in the ZOF). These changes are also the key factors controlling the heterogeneous Mesozoic mineralization in the SCB.

5.5. Implications of the spatial coincidence of the Sn-W and Mo-Cu/Cu-Mo mineralizations

As mentioned above, Sn(W) has geochemical behaviors that are distinctly different than those of Mo and especially Cu; therefore, Sn-W and Mo-Cu mineralizations usually occur in distinct belts and seldom temporally-spatially coincide.

A model of two-step melting has been suggested to explain the local superposition of the Sn and/or W mineralization with the Cu and/or Mo mineralization, i.e., early preferential melting of sedimentary rocks to form reduced Sn-rich melts, followed by more oxidized Cu-Mo rich melts after the sedimentary protoliths are consumed (Romer and Kroner, 2016). The two-step melting would form Sn and/or W deposits slightly older than the Cu and/or Mo deposits, rather than cause the spatial-temporal overlap of these two groups of mineralizations. In our study, we propose that the superposition of the simultaneously produced Mo-Cu porphyry and granite-related Sn deposits is controlled by high temperature melting of crustal protoliths with different lithologies. Melting of a meta-sedimentary protolith formed the reduced and Sn-W-rich magma, whereas melting of a meta-basaltic protolith formed the oxidized and Mo-Cu-rich magma. Thus, melting of mature crust containing various protoliths combined with heat from the mantle

provides an alternative explanation for the temporal-spatial coincidence of the Mo-Cu and Sn-W mineralizations.

Overall, the metal associations and spatial distribution of the intrusion related deposits are controlled by their source components and heat supply. The spatial and temporal coincidence of the Sn-W and Cu-Mo-(Au) mineralizations are primarily controlled by high temperature crustal melting caused by the same dynamic processes. The spatially overlapping but diachronous Sn-W and Cu-Mo-(Au) mineralizations reflect changes in the source components and geodynamic background, which suggests a shift in the tectonic framework.

6. Conclusions

The main findings of this study are summarized as follows.

(1) The adjacent Jurassic ZJS Sn-related granites and Gutian Mo-Cu-related porphyry formed ~155–165 Ma in the coastal region of southeastern China and were derived from meta-sedimentary rocks and meta-basaltic rocks, respectively.
(2) The Jurassic Sn mineralized granite and the Mo-Cu mineralized porphyry in the coastal region of southeastern China were formed in the same tectonic setting as the Jurassic Sn-W granites in the Nanling Range, and the mineralization in both locations was triggered by hinterland extension and asthenospheric upwelling.
(3) The transition in the tectonic setting is responsible for the spatial superposition of the Cretaceous Cu-Mo porphyry deposit and the Jurassic Sn and Mo-Cu mineralizations in SE China.
(4) Partial melting of different protoliths and a transition in the tectonic setting, which could result in changes in the magmatic source, water concentration, oxidization, and evolution path, triggered the simultaneous and diachronous superposition of the Sn(W) and Mo-Cu deposits.

Declaration of Competing Interest

None.

Acknowledgments

This study was supported by the National Natural Science Foundation of China (42072088 and 41502073). We would like to thank the Geological Department of the Zijin Mining Company for their assistance during field work. We thank editor Prof. Xianhua Li, Rui Wang, and an anonymous reviewer for their detailed comments and suggestions which improved the artile to higher level.This is contribution No.IS-2920 from GIGCAS.

Appendix A. Supplementary data

Supplementary data to this article can be found online at https://doi.org/10.1016/j.lithos.2020.105816.

References

Audétat, A., 2010. Source and evolution of molybdenumin the porphyry Mo(–Nb) deposit at Cave Peak, Texas. J. Petrol. 51, 1739–1760.
Beard, J.S., Lofgren, G.E., 1991. Dehydration melting and water-saturated melting of basaltic and andesitic greenstones and amphibolites at 1, 3, and 6.9kb. J. Petrol. 32, 365–401.
Chen, J.F., Jahn, B.M., 1998. Crustal evolution of southeastern China: evidence from Sr, Nd and Pb isotopic compositions of granitoids and sedimentary rocks. Tectonophysics 284 (101–133).
Chen, C.H., Lee, C.Y., Shinjo, R., 2008. Was there Jurassic paleo-Pacific subduction in South China?: constraints from $^{40}Ar/^{39}Ar$ dating, elemental and Sr–Nd–Pb isotopic geochemistry of the Mesozoic basalts. Lithos 106, 83–92.
Chen, R.S., Li, J.W., Cao, K., Qu, C.Y., Li, Y.J., 2013. Zircon U-Pb and molybdenite Re-Os dating of the Shangfang tungsten deposit in northern Fujian Province: implications for regional mineralization (in Chinese with English abstract). Earth Science-Journal of China University of Geosci 38(2), 289–304.
Chen, Y., Li, H., Sun, W., Ireland, T., Tian, X., Hu, Y., Yang, W., Chen, C., Xu, D., 2016. Generation of late Mesozoic Qianlishan A2-type granite in Nanling Range, South China: implications for Shizhuyuan W–Sn mineralization and tectonic evolution. Lithos 266-267, 435–452.
Clark, C., Fitzsimmons, I.C.W., Healy, D., 2011. How does the continental crust get really hot? Elements 7, 235–240.
Collins, W.J., Huang, H.Q., Jiang, X.Y., 2016. Water-fluxed crustal melting produces Cordilleran batholiths. Geology (2), 143–146.
Cooke, D.R., Hollings, P., Walsh, J.L., 2005. Giant porphyry deposits: characteristics, distribution, and tectonic controls. Econ. Geol. 100 (5), 801–818.
Garson, M.S., Mitchell, A.H.G., 1977. Mineralization at destructive plate boundaries: a brief review. Geol. Soc. Lond. Spec. Publ. 7, 81–97.
Gilder, S.A., Keller, G.R., Luo, M., Goodell, P.C., 1991. Timing and spatial-distribution of rifting in China. Tectonophysics 197, 225–243.
Guo, F., Fan, W.M., Li, C.W., Zhao, L., Li, H.X., Yang, J.H., 2012. Multi-stage crust-mantle interaction in SE China: temporal, thermal and compositional constraints from the Mesozoic felsic volcanic rocks in eastern Guangdong-Fujian provinces. Lithos 150, 62–84.
Heinrich, C.A., 1990. The chemistry of hydrothermal tin (−tungsten) ore deposition. Econ. Geol. 85, 457–481.
Hollings, P., Cooke, D., Clark, A., 2005. Regional geochemistry of Tertiary igneous rocks in Central Chile: implications for the geodynamic environment of giant porphyry copper and epithermal gold mineralization. Econ. Geol. 100, 887–904.
Hou, Z., Ma, H., Khin, Z., Zhang, Y., Wang, M., Wang, Z., Pan, G., 2003. The Himalayan Yulong porphyry copper belt; product of largescale strike–slip faulting in eastern Tibet. Econ. Geol. 98, 125–145.
Hu, R.Z., Zhou, M.F., 2012. Multiple Mesozoic mineralization events in South China-an introduction to the thematic issue. Miner. Deposita 47, 579–588.
Huang, H.Q., Li, X.H., Li, Z.X., Li, W.X., 2015. Formation of the Jurassic South China Large Granitic Province: Insights from the genesis of the Jiufeng pluton. Chemical Geology 401, 43–58.
Huang, W., Li, J., Wang, C., Lin, S., Wang, X., 2013. Zircon LA-ICP-MS U-Pb ages and highly oxidized factures of magma associated with Luoboling porphyry Cu-Mo deposit in Zijinshan ore field, Fujian Province. Acta Petrol. Sin. 29 (1), 282–293 (in Chinese with English abstract).
Huang, W., Liang, H.Y., Wu, J., Zou, Y.Q., Zhang, J., 2017a. Formation of porphyry Mo deposit in a deep fault zone, example from the Dabaoshan porphyry Mo deposit in northern Guangdong, South China. Ore Geol. Rev. 81, 940–952.
Huang, W., Wu, J., Zhang, J., Liang, H.Y., Qiu, X.L., 2017b. Geochemistry and Hf–Nd isotope characteristics and forming processes of the Yuntoujie granites associated with W–Mo deposit, Guangxi, South China. Ore Geol. Rev. 81, 953–964.
Huang, W.T., Liang, H.Y., Wu, L., Wu, J., Li, J., Bao, Z.W., 2018. Asynchronous formation of the adjacent epithermal Au-Cu and porphyry Cu-Mo deposits in the Zijinshan orefield, Southeast China. Ore Geol. Rev. 102, 351–367.
Irber, W., 1999. The lanthanide tetrad effect and its correlation with K/Rb, Eu/Eu*, Sr/Eu, Y/Ho, and Zr Hf of evolving peraluminous granite suites. Geoch. Cosmoch. AC 63, 489–508.
Ishihare, S., 1981. The Granitoid Series and Mineralization. Economic Geology, 75th Anniversary Volume. pp. 458–484.
Jiang, S.H., Liang, Q.L., Bagas, L., Wang, S.H., Nie, F.J., Liu, Y.F., 2013. Geodynamic setting of the Zijinshan porphyry–epithermal Cu–Au–Mo–Ag ore system, SW Fujian Province, China: constrains from the geochronology and geochemistry of the igneous rocks. Ore Geol. Rev. 53, 287–305.
Jugo, P.J., 2009. Sulfur content at sulfide saturation in oxidized magmas. Geology 37, 415–418.
Lehmann, B., 2004. Metallogeny of the Central Andes: Geotectonic framework and geochemical evolution of porphyry systems in Bolivia and Chile during the last 40 million years. In: Khanchuk, A.I., Gonevchuk, G.A., Mitrokhin, A.N., Simanenko, L.F., Cook, N.J., Seltmann, R. (Eds.), Metallogeny of the Pacific Northwest: Tectonics, Magmatism and Metallogeny of Active Continental Margins. Vladivostok Dalnauka, Proceedings of the Interim JAGOD Conference, Vladivistok/Russia, pp. 118–122.
Li, X.H., Sun, M., Wei, G.J., Lee, C.Y., Malpas, J., 2000. Geochemical and Sm±Nd isotopic study of amphibolites in the Cathaysia Block, southeastern China: evidence for an a extremely depleted mantle in the Paleoproterozoic. Precambrian Research 102, 251–262.
Li, B., Zhao, K.D., Zhang, Q., Xu, Y.M., Zhu, Z.Y., 2015. Petrogenesis and geochemical characteristics of the Zijinshan granitic complex from Fujian Province, South China. Acta Petrol. Sin. 31 (3), 811–828 (in Chinese with English abstract).
Li, Y., Audétat, A., 2012. Partitioning of V, Mn, Co, Ni, Cu, Zn, As, Mo, Ag, Sn, Sb, W, Au, Pb, and Bi between sulfide phases and hydrous basanite melt at upper mantle conditions. Earth and Planetary Science Letters 355-356, 327–340.
Li, B., Jiang, S.Y., Lu, A.H., Lai, J.Q., Zhao, K.D., Yang, T., 2016a. Petrogenesis of late Jurassic granodiorites from Gutian, Fujian Province, South China: Implications for multiple magma sources and origin of porphyry Cu–Mo mineralization. Lithos 264, 540–554.
Li, B., Jiang, S.Y., Zhang, Q., Zhao, H.X., Zhao, K.D., 2016b. Geochemistry, geochronology and Sr–Nd–Pb–Hf isotopic compositions of middle to late Jurassic syenite–granodiorites–dacite in South China: petrogenesis and tectonic implications. Gondwana Res. 35, 217–237.
Li, X.H., 2000. Cretaceous magmatism and lithospheric extension in Southeast China. J. Asian Earth Sci. 18 (3), 293–305.
Li, X.H., Li, Z.X., Li, W.X., Wang, X.C., Gao, Y., 2013. Revisiting the "C-type adakites" of the lower Yangtze River Belt, central eastern China: In-situ zircon Hf–O isotope and geochemical constraints. Chem. Geol. 345, 1–15.

Li, Z., Qiu, J.-S., Yang, X.M., 2014. A review of the geochronology and geochemistry of late Yanshanian (cretaceous) plutons along the Fujian coastal area of southeastern China: Implications for magma evolution related to slab break-off and rollback in the cretaceous. Earth-Sci. Rev. 128, 232–248.
Li, Z.X., Li, X.H., 2007. Formation of the 1300-km-wide intracontinental orogen and postorogenic magmatic province in Mesozoic South China: a flat-slab subduction model. Geology 35 (2), 179–182.
Liang, H.Y., Campbell, I.H., Allen, C., Sun, W.D., Liu, C.Q., Yu, H.X., Xie, Y.W., Zhang, Y.Q., 2006. Zircon Ce^{4+}/Ce^{3+} ratios and ages for Yulong ore-bearing porphyries in eastern Tibet. Mineral. Deposita 41, 152–159.
Liang, H.Y., Sun, W.D., Ling, M.X., Ding, X., Yang, X., 2009. Porphyry Cu (Au) deposit promoted by redox decoupling during magnetite alteration in Yulong. Geochim. Cosmochim. Acta 73 (13), A761.
Linnen, R.L., 1998. Depth of emplacement, fluid provenance and metallogeny in granitic terranes: a comparison of western Thailand with other tin belts. Mineral. Deposita 33, 461–476.
Linnen, R.L., Pichavant, M., Holtz, F., Burgess, S., 1995. The effects of fO_2 on the solubility, diffusion, and speciation of tin in haologranitic melt at 850 C and 2kbar. Geochim. Cosmochim. Acta 59, 1579–1588.
Liu, W.Y., Nigel, C.J., Cristiana, C.L., Liu, Y., Qiu, X.P., Chen, Y.Q., 2016. Mineralogy of tin-sulfides in the Zijinshan porphyry–epithermal system, Fujian Province, China. Ore Geol. Rev. 72, 682–698.
Mao, J.W., Cheng, Y.B., Chen, M.H., Franco, P., 2013. Major types and time–space distribution of Mesozoic ore deposits in South China and their geodynamic settings. Mineral. Deposita 48, 267–294.
McDonough, W.F., Sun, S.S., 1995. The composition of the Earth. Chemical Geology 120, 223–253.
Mitchell, A.H.G., 1973. Metallogenic belts and angle of dip of Benioff zones. Nature 245, 49–52.
Mitchell, A.H.G., Garson, M.S., 1981. Mineral Deposits and Global Tectonic Settings. Academic Press, London, p. 405.
Monecke, T., Kempf, U., Monecke, J., Sala, M., Wolf, D., 2002. Tetrad effect in rare earth element distribution patterns: a method of quantification with application to rock and mineral samples from granite-related rare metal deposits. Geoch. Cosmoch. AC 66, 1185–1196.
Qiu, Z., Li, S., Yuan, Q., Wang, H., Wei, X., Li, P., Wang, L., Bu, A., 2017. Late Jurassic Sn metallogeny in eastern Guangdong, SE China coast: Evidence from geochronology, geochemistry and Sr–Nd–Hf–S isotopes of the Dadaoshan Sn deposit. Ore Geology Reviews 83 (63-).
Richards, J.P., 2003. Tectono-magmatic precursors for porphyry Cu-(Mo-Au) deposit formation. Economic Geology and the Bulletin of the Society of Economic Geologists 8, 1515–1533.
Richards, J.P., 2009. Postsubduction porphyry Cu–Au and epithermal Au deposits: products of remelting of subduction-modified lithosphere. Geology 37, 247–250.
Richards, J.P., 2011. Magmatic to hydrothermal metal fluxes in convergent and collided margins. Ore Geol. Rev. 40, 1–26.
Richards, J.P., Spell, T., Rameh, E., Razique, A., Fletcher, T., 2012. High Sr/Y magmas reflect arc maturity, high magmatic water content, and porphyry Cu ± Mo ± Au potential: examples from the tethyan arcs of central and eastern Iran and western Pakistan. Econ. Geol. 107 (2), 295–332.
Romer, R.L., Kroner, U., 2015. Sediment and weathering control on the distribution of Paleozoic magmatic tin¨Ctungsten mineralization. Mineral. Deposita 50, 327–338.
Romer, R.L., Kroner, U., 2016. Phanerozoic tin and tungsten mineralization-Tectonic controls on the distribution of enriched protoliths and heat sources for crustal melting. Gondwana Res. 31, 60–95.
Rudnick, R.L., Gao, S., 2003. Composition of the continental crust. In: Rudnick, R.L. (Ed.), Treatise on Geochemistry 3: The Crust. Elsevier, Amsterdam, pp. 1–64.
Sato, K., Kovalenko, S.V., Romanovsky, N.P., Nedachi, M., Berdnikov, N.V., Ishihara, T., 2004. Crustal control on the redox state of granitoid magmas: tectonic implications from the granitoid and metallogenic provinces in the circum-Japan Sea Region. Geol. Soc. Am. Spec. Pap. (389), 319–337.
Shen, W.Z., 2006. Comment on the isotopic age data of basemenet metamorphic rocks in Cathaysia Block. Geol. J. China Univ. 12, 475–482.
Shu, L.S., Zhou, X.M., Deng, P., Yu, X.Q., Wang, B., Zu, F.P., 2004. Geological features and tectonic evolution of Mes-Cenozoic basins in southeastern China. Geol. Bull. China 23, 876–884 (in Chinese with English abstract).
Sillitoe, R.H., 1972. A plate tectonic model for the origin of porphyry copper deposits. Econ. Geol. 67, 184–197.
Sillitoe, R.H., 1974. Tin mineralisation above mantle hot spots. Nature 248, 497–499.
Sillitoe, R.H., 2010. Porphyry copper systems. Econ. Geol. Bull. Soc. Econ. Geol. 105, 3–41.
So, C.S., Zhang, D.Q., Yun, S.T., Li, D.X., 1998. Alteration-mineralization zoning and fluid inclusions of the high sulfidation epithermal Cu-Au mineralization at Zijinshan, Fujian province, China. Econ. Geol. 93, 961–980.
Sun, T., 2006. A new map showing the distribution of granites in South China and ite explanatory notes. Geol. Bull. China 25 (3), 332–335 (in Chinese with English abstract).
Sun, W.D., Ding, X., Hu, Y.H., Li, X.H., 2007. The golden transformation of the cretaceous plate subduction in the West Pacific. Earth Planet. Sci. Lett. 262, 533–542.
Sun, W.D., Liang, H.Y., Ling, M.X., Zhan, M.Z., Ding, X., Zhang, H., Yang, X.Y., Li, Y.L., Ireland, T.R., Wei, Q.R., 2013. The link between reduced porphyry copper deposits and oxidized magmas. Geochim. Cosmochim. Acta 103, 263–275.
Sylvester, P.J., 1998. Post-collisional strongly peraluminous granites. Lithos 45, 29–44.
Thomas, R., Davidson, P., 2013. The missing link between granites and granitic pegmatites. J. Geosci. 58, 193–200.
Thomas, R., Webster, J.D., Heinrich, W., 2000. Melt inclusions in pegmatite quartz: complete miscibility between silicatemelts and hydrous fluids at low pressure. Contrib. Mineral. Petrol. 139, 394–401.
Thomas, R., Förster, H.J., Rickers, K., Webster, J.D., 2005. Formation of extremely F-rich hydrous melt fractions and hydrothermal fluids during differentiation of highly evolved tin-granitemagmas: amelt/fluid-inclusion study. Contrib. Mineral. Petrol. 148, 582–601.
Wang, R., Tafti, R., Hou, Z.Q., Shen, Z.C., Guo, N., Evans, N.J., Jeon, H., Li, Q.Y., Li, W.K., 2017. Across-arc geochemical variation in the Jurassic magmatic zone, Southern Tibet: Implication for continental arc-related porphyry Cu-Au mineralization. Chem. Geol. 451, 116–134.
Wang, Y.J., Fan, W.M., Peter, A., Cawood, Li S.Z., 2008. Sr-Nd-Pb isotopic constraints on multiple mantle domains for Mesozoic mafic rocks beneath the South China Block. Lithos 106, 297–308.
Wang, Y.J., Fan, W.M., Zhang, G.W., Zhang, Y.H., 2013. Phanerozoic tectonics of the South China Block: key observations and controversies. Gondwana Res. 23 (4), 1273–1305.
Watson, E.B., Harrison, T.M., 1983. Zircon saturation revisited: temperature and composition effects in a variety of crustal magma types. Earth Planet. Sci. Lett. 64, 295–304.
Weinberg, R.F., Hasalová, P., 2015. Water-fluxed melting of the continental crust: a review. Lithos 212-215, 158–188.
Williams-Jones, A.E., Heinrich, C.A., 2005. Vapor transport of metals and the formation of magmatic-hydrothermal ore deposits. Econ. Geol. 100, 1287–1312.
Xia, Y., Xu, X.S., Zhu, K.Y., 2012. Paleoproterozoic S- and A-type granites in southwestern Zhejiang: Magmatism, metamorphism and implications for the crustal evolution of the Cathaysia basement. Precambrian Research 216-219, 177–207.
Xie, D.K., Ma, R.S., Zhang, Y.S., Zhao, X.X., Coe, R.S., 1996. The Crust Growth and Mantle Plume Tectonics of South China Continent. Geological Publishing House, Beijing, pp. 1–257 (in Chinese with English abstract).
Xu, X., O'Reilly, S.Y., Griffin, W.L., Wang, X., Pearson, N.J., He, Z., 2007. The crust of Cathaysia: age, assembly and reworking of two terranes. Precambrian Res. 158, 51–78.
Yu, B., Pei, R.F., Qiu, X.P., Chen, J.H., Li, D.P., Zhang, W.H., Liu, W.Y., 2013. The evolution series of mesozoic magmatic rocks in the Zijinshan Orefield, Fujian Province. Acta Geol. Sin. 34, 437–446 (in Chinese with English abstract).
Yu, J.H., Wang, L.J., O'Reilly, S.Y., Griffin, W.L., Zhang, M., Li, C.Z., Shu, L.S., 2009. A Paleoproterozoic orogeny recorded in a long-lived cratonic remnant (Wuyishan terrane), eastern Cathaysia Block, China. Precambrian Research 174, 347–363.
Yuan, S., Williams-Jones, A.E., Romer, R.L., Zhao, P., Mao, J.W., 2019. Protolith-related thermal controls on the decoupling on Sn and W in Sn-W metallogenic provinces: insights from the Nanling Region, China. Econ. Geol. 114, 1005–1012.
Zajacz, Z., Halter, W.E., Pettke, T., Guillong, M., 2008. Determination of fluid/melt partition coefficients by LA-ICPMS analysis of co-existing fluid and silicate melt inclusions: controls on element partitioning. Geochim. Cosmochim. Acta 72, 2169–2197.
Zhang, D.Q., Li, D.X., Feng, C.Y., Dong, Y.J., 2001. The temporal and spatial framework of the mesozoic magmatic system in zijinshan area and its geological significance. Acta Geosci. Sin. 22, 403–408.
Zhang, J., Chen, Z., Wang, D., Chen, Z., Liu, S., Wang, C., 2008. Geological characteristics and metallogenic epoch of the Xingluokeng tungsten deposit, Fujian province. Geotecton. Metallog. 32, 92–97 (in Chinese with English abstract).
Zhang, J.J., 2013. Geology, exploration model and practice of Zijinshan ore concentrated area. Mineral. Deposita 32, 757–766 (in Chinese with English abstract).
Zhang, W.L., Wang, R.C., Hua, R.M., 2006. Study of a series of Ta-minerals in Dajishan W-Nb-Ta deposit, South China. Geochim. Cosmochim. Acta 70, 739.
Zhao, X.L., Mao, J.R., Chen, R., Xu, N.Z., Zeng, Q.T., Ye, H.M., 2007. Zircon SHRIMP age and geochemical characteristics of the Caixi pluton in southwestern Fujian Province. Acta Petrol. Mineral. 26, 223–231 (in Chinese with English abstract).
Zhong, J., Chen, Y.J., Pirajno, F., Chen, J., Li, J., Qi, J.P., Li, N., 2014. Geology, geochronology, fluid inclusion and H–O isotope geochemistry of the Luoboling Porphyry Cu–Mo deposit, Zijinshan Orefield, Fujian Province, China. Ore Geol. Rev. 57, 61–77.
Zhou, X.M., Li, W.X., 2000. Origin of late Mesozoic igneous rocks in Southeastern China: implications for lithosphere subduction and underplating of mafic magmas. Tectonophysics 326, 269–287.
Zou, Y., Chen, X., Huang, W., Zhang, J., Liang, H., Xu, J., Chen, L., 2017. Identification of an early–middle jurassic oxidized magmatic belt, south Gangdese, Tibet, and geological implications. Sci. Bull. 62, 888–898.